Mon. Not. R. Astron. Soc. **000**, 1–?? (2005) Printed 7 April 2012 (MN LATEX style file v2.2)

Astrometric and photometric initial mass functions from the UKIDSS Galactic Clusters Survey: I The Pleiades ⋆

N. Lodieu[1,2]†, N. R. Deacon[3], N. C. Hambly[4]
[1]*Instituto de Astrofísica de Canarias (IAC), Vía Láctea s/n, E-38205 La Laguna, Tenerife, Spain*
[2] *Departamento de Astrofísica, Universidad de La Laguna (ULL), E-38205 La Laguna, Tenerife, Spain*
[3]*Max-Planck-Institut für Astronomie, Königstuhl 17, 69117, Heidelberg, Germany*
[4]*Scottish Universities' Physics Alliance (SUPA), Institute for Astronomy, School of Physics, University of Edinburgh, Royal Observatory, Blackford Hill, Edinburgh EH9 3HJ, UK*

Accepted 7 April 2012. Received 7 April 2012; in original form 7 April 2012

ABSTRACT
We present the results of a deep wide-field near-infrared survey of the entire Pleiades cluster recently released as part of the UKIRT Infrared Deep Sky (UKIDSS) Galactic Clusters Survey (GCS) Data Release 9 (DR9). We have identified a sample of ∼1000 Pleiades cluster member candidates combining photometry in five near-infrared passbands and proper motions derived from the multiple epochs provided by the UKIDSS GCS DR9. We also provide revised membership for all previously published Pleiades low-mass stars and brown dwarfs in the past decade recovered in the UKIDSS GCS DR9 Pleiades survey based on the new photometry and astrometry provided by the GCS. We find no evidence of K-band variability in the Pleiades members larger than $\sim$ 0.08 mag. In addition, we infer a substellar binary frequency of 22–31% in the 0.075–0.03 $M_{\odot}$ range for separations less than ∼100 au. We employed two independent but complementary methods to derive the cluster luminosity and mass functions: a probabilistic analysis and a more standard approach consisting of stricter astrometric and photometric cuts. We found that the resulting luminosity and mass functions obtained from both methods are very similar. We derive the Pleiades mass function in the 0.6–0.03 $M_{\odot}$ mass range and found that it is best reproduced by a log-normal representation with a mean characteristic mass of 0.20±0.05 $M_{\odot}$, in agreement with earlier studies and the extrapolation of the field mass function.

Key words: Techniques: photometric — stars: low-mass, brown dwarfs; stars: luminosity function, mass function — galaxy: open clusters and associations: individual (Pleiades) — infrared: stars

1 INTRODUCTION

Over the past two decades star forming regions and rich, young open clusters have been the focal points of numerous searches for substellar objects in the form of wide-field or pencial-beam surveys (e.g. Jameson & Skillen 1989; Hambly et al. 1993; Luhman 1999; Lucas & Roche 2000; Béjar et al. 2001; Zapatero Osorio et al. 2002; Tej et al. 2002; Moraux et al. 2003; Lodieu et al. 2006, 2007). Among the key milestones in the study of substellar objects, we should point out the discovery of a first brown dwarf in a star-forming region (ρ Oph; Luhman et al. 1997), the identification of young L dwarfs (Martín et al. 1998), and the first young T dwarf member of σ Orionis (SOri 70; Zapatero Osorio et al. 2002). The common scientific driver of these surveys in young regions is the study of the Initial Mass Function (IMF; Salpeter 1955; Miller & Scalo 1979; Scalo 1986; Kroupa 2002; Chabrier 2005) and its possible universality through the imaging and spectroscopic confirmation of candidate members in a wide variety of environments.

The UKIRT Infrared Deep Sky Survey (UKIDSS; Lawrence et al. 2007)[1] is a deep large-scale infrared survey. All photometric observations, obtained with the Wide field CAMera (WFCAM; Casali et al. 2007) equipped with five infrared filters ($ZYJHK$; Hewett et al. 2006), are pipeline-processed at the Cambridge Astronomical Survey Unit (CASU; Irwin et al. 2007, Irwin et al. in preparation)[2]. The processed data are then archived in Edinburgh and released to the user community through the WFCAM Science

⋆ Based on observations made with the United Kingdom Infrared Telescope, operated by the Joint Astronomy Centre on behalf of the U.K. Particle Physics and Astronomy Research Council.
† E-mail: nlodieu@iac.es

[1] The survey is described at www.ukidss.org
[2] The CASU WFCAM-dedicated webpage can be found at http://apm15.ast.cam.ac.uk/wfcam

Archive (WSA; Hambly et al. 2008)[3]. One of its components, the Galactic Clusters Survey (hereafter GCS) aims at covering ∼1000 square degrees in 10 star-forming regions and open clusters down to 0.03–0.01 $M_{\odot}$ (depending on the age and distance) to investigate the universality of the initial mass function. Each cluster is covered in $ZYJHK$ with a second epoch in K to provide proper motions with accuracies of a few milli-arcsec per year (mas/yr). The latest GCS data release (DR) to date, DR9 on 25 October 2011, provides full coverage of the Pleiades in those five filters along with proper motions. This paper is the first of a series dedicated to the astrometric and photometric mass functions in young and intermediate-age open clusters as well as star-forming regions to address the fundamental issue of the universality of the IMF in an homogeneous manner.

The rich Pleiades cluster has been subjected to a particularly high degree of scrutiny for several reasons. First, its members share a significant common proper motion compared to neighbouring stars estimated to ($\mu_{\alpha} \cos \delta$, μ_{δ}) = (+19.15, −45.72) and (+20.10, −45.39) mas/yr by Robichon et al. (1999) and van Leeuwen (2009) respectively, making astrometric selection relatively straightforward. Furthermore, the Pleiades is among the nearest well-populated open clusters located at 134 pc from the Sun with an uncertainty of 5 pc (Johnson 1957; Gatewood et al. 2000; Pinfield et al. 2000; Southworth et al. 2005) while the improved reduction of the Hipparcos data by van Leeuwen (2009) suggests a distance of 120.2±1.9 pc. In this work we adopt this latter estimate. Its age has been determined using various methods, including the Zero-Age-Main-Sequence turn-off (Mermilliod 1981) and the lithium depletion boundary methods (Stauffer et al. 1998). The latter method yielded a most probable value of 125 ± 8 Myr. Moreover, reddening along the line of sight to the cluster is generally low, E($B-V$) = 0.03 (O'dell, Hendry & Collier Cameron 1994). Finally, the number of Pleiades members is large due to the numerous surveys dedicated to the stellar and substellar components of the cluster (Jameson & Skillen 1989; Hambly et al. 1993; Stauffer et al. 1994; Zapatero Osorio et al. 1997; Stauffer et al. 1998; Martín et al. 1998; Bouvier et al. 1998; Festin 1998; Zapatero Osorio et al. 1999; Hambly et al. 1999; Pinfield et al. 2000; Adams et al. 2001; Moraux et al. 2001; Jameson et al. 2002; Dobbie et al. 2002; Moraux et al. 2003; Deacon & Hambly 2004; Bihain et al. 2006, 2010; Casewell et al. 2007; Lodieu et al. 2007; Bihain et al. 2010; Casewell et al. 2011).

In this paper we present the Pleiades mass function derived from ∼80 square degrees surveyed in 5 passbands, one at 2 epochs, by the UKIDSS GCS to provide photometry and astrometry for about one million sources. These data come from the latest data release of the UKIDSS GCS, DR9. In Section 2 we present the photometric and astrometric dataset employed to extract Pleiades member candidates. In Section 3 we review the list of previously published members recovered by the UKIDSS GCS DR9 and revise their membership. In Section 4 we outline two methods for deriving the cluster luminosity function. One method relies on a relatively conservative photometric selection followed by the calculation of formal membership probabilities based on objects positions in the proper motion vector point diagram (Section 4.1). The second method applies a rigorous astrometric selection based on the formal errors on the proper motions for each photometric candidate compared to the mean of the cluster (Section 4.2) after more stringent multicolour cuts. In Section 5 we discuss the photometric binary frequency in the substellar regime and compare it with previous estimates in the Pleiades and for ultracool field dwarfs. In Section 6 we discuss the K-band variability of Pleiades cluster member candidates. In Section 7 we derive the cluster luminosity and (system) mass function and compare it to earlier estimates for this cluster and others, along with that of the field population.

[3] The WFCAM Science Archive is accessible at the URL http://surveys.roe.ac.uk/wsa

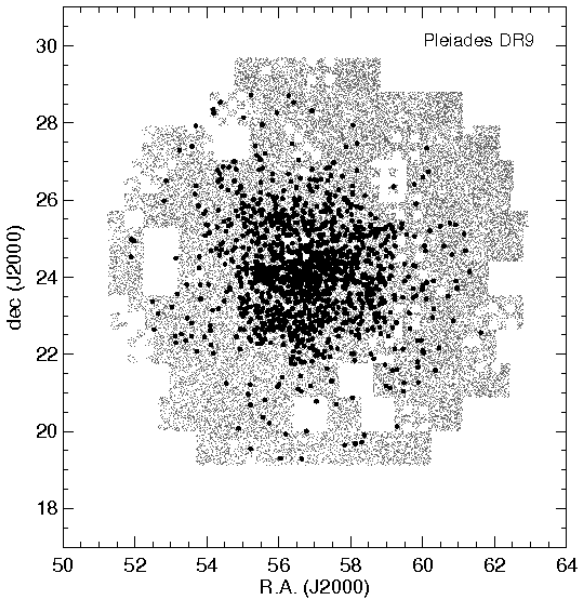

Figure 1. The coverage in the Pleiades as released by the UKIDSS GCS DR9 (grey region). The holes are due to frames removed from the GCS release due to quality control issues. Overplotted are previously known member candidates recovered by the GCS DR9 (filled black dots).

2 THE ASTROMETRIC AND PHOTOMETRIC DATASET

2.1 Photometry

We selected point sources in the full Pleiades cluster, in the region defined by RA=50–64 degrees and dec=18–30 degrees. We retrieved the catalogue using a Structure Query Language (SQL) query similar to our earlier study of the Pleiades (Lodieu et al. 2007) and applied it to the DR9 release of the GCS (see also the SQL query in appendix A of Lodieu et al. (2007)).

Briefly, we selected only good quality point sources in all passbands and included Z and Y non detections to allow for cooler brown dwarf candidates to be extracted. We did not impose a detection in the second K-band either because the proper motions are not only computed with the two K-band epochs but with any filter observed at a different time (see Section 2.2). We limited our selection to sources fainter than Z = 11.3, Y = 11.5, J = 11.0, H = 11.3, and $K1$ = 9.9 mag where the GCS saturates. The completeness limits, taken as the magnitude where the straight line fitting the shape of the number of sources as a function of magnitudes falls off, are Z = 20.2, Y = 19.8, J = 19.3, H = 18.4, $K1$ = 17.9, and $K2$ = 18.1 mag (Fig. 2). The SQL query includes a cross-match with the Two Micron All Sky Survey (2MASS; Cutri et al. 2003; Skrutskie et al. 2006) if available. The main change here compared to our previous study of the Pleiades made with the GCS DR1, apart from the significant increase in areal coverage, is the inclusion of

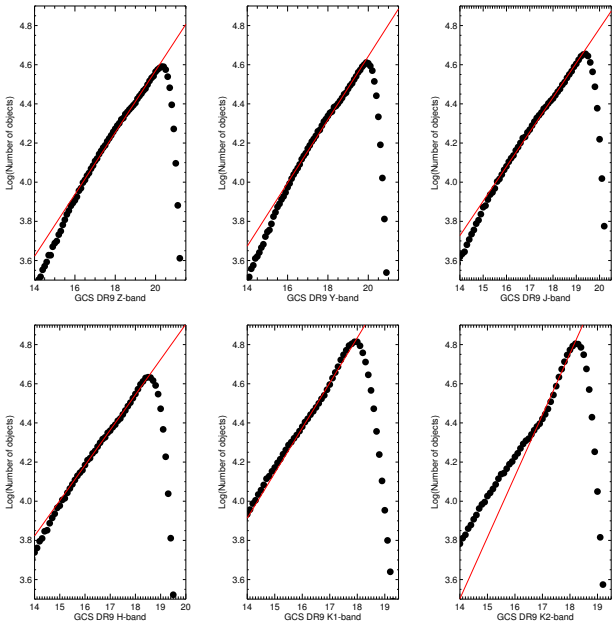

Figure 2. Completeness of the GCS DR9 dataset in the Pleiades cluster in each of the six filters. The polynomial fit of order 2 is shown as a red and defines the 100% completeness limit of the GCS DR9 in each passband.

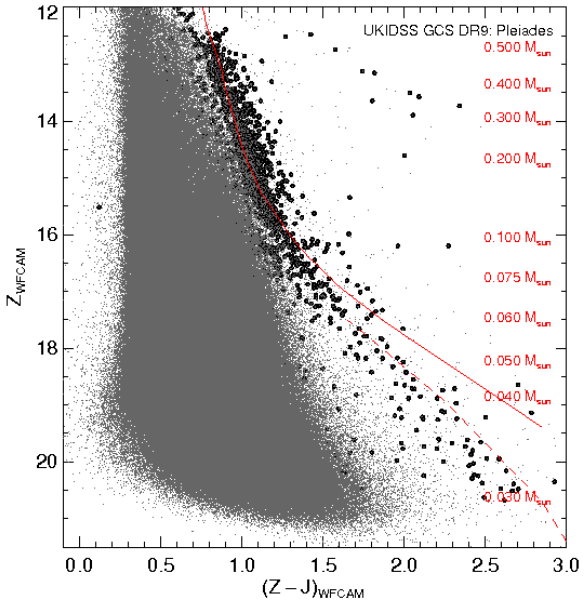

Figure 3. $(Z-J,Z)$ CMD for $\sim$80 square degrees in the Pleiades extracted from the UKIDSS Galactic Cluster Survey Data Release 9. Previously published Pleiades member candidates are overplotted as filled dots. The mass scale is shown on the right hand side of the diagram and extends down to $\sim$0.02 $M_{\odot}$, according to the NextGen (solid line) and DUSTY (dashed line) models (Baraffe et al. 1998; Chabrier et al. 2000).

the proper motions determined from the multiple passband coverage taken at different epochs by the GCS and released in DR9 (see Section 2.2 for more details). The query returned a total of 937,723 sources over $\sim$80 square degrees. The full coverage is displayed in Fig. 1 and the resulting $(Z-J,Z)$ colour-magnitude diagram is shown in Fig. 3. We note that the theoretical isochrones plotted in the different figures of the paper were specifically computed for the WFCAM set of filters and kindly provided by I. Baraffe and F. Allard.

2.2 Astrometry

Proper motion measurements are available in the WFCAM Science Archive for UKIDSS data releases from DR9 for all the wide/shallow surveys with multiple epoch coverage in each field (i.e. the LAS, GCS and GPS). Details of the procedure will appear elsewhere (Collins & Hambly 2012), but here we give a brief description of the process.

When complete, each field imaged in the UKIDSS surveys is covered by a set of detector frames in various passbands with one passband revisited at least once. In general, these frames may have been taken at any time over the lifetime of the survey (at the time of writing, $\sim$ 6 years) resulting in multiple epoch coverage for all sources. The approach taken in the WSA for computing proper motions is simple[4]: first a set of local plane coordinates was established for all detections in all frames that have any systematic offsets in absolute positions minimised; then proper motions were measured from linear least–squares fits in these local plane coordinates as a function of time. In the first process, for each set of frames, one reference frame was taken to map each other 'slave' frame onto that master using *all* available detections and a simple linear 'plate' model. Working in local plane coordinates, the model comprises 6 coefficients allowing for independent zeropoint shifts and scale changes in both coordinates, rotation and non–orthogonality between the coordinate axes (shear). The reason for applying these local models is that the absolute astrometry of each frame is done with respect to relatively bright 2MASS standard stars, so the zeropoint of any proper motions derived by simply taking these raw positions would be defined by these relatively nearby stars, and would be subject to any bulk motions and/or drift of such stars as seen from our vantage point in space. The idea was to define a zeropoint for the proper motions across all surveys that is as close as possible to a true zero, i.e. one in which the average galaxy and quasar proper motions would be zero. Clearly this is not possible in low–latitude sightlines and/or for relatively shallow detection lists containing few identified extragalactic sources, so the best that can be done is to use the faintest and hence on average most distant stars possible. Since the number counts are dominated by the fainter stars, all stars were simply used. Note that rather than weighting these local model fits by the formal errors on each detection, unit–weight fits were chosen. Again, this is because the brighter, and on average nearer stars would carry the most weight given their low centroiding errors, but the local mapping models should not be biased towards the possibly drifting reference frame that would be defined by such stars which exhibit significant angular motions simply because of their proximity to the Sun.

Once a set of mapped local plane coordinates was set for every source paired across the detections available from the set of frames, a weighted linear least–squares fit is done for each coordinate as a function of time, resulting in four astrometric parameters (coordinates at a reference epoch along with proper motions in those

[4] we emphasise that this work was done within the WSA for all the UKIDSS wide/shallow surveys, and not carried out for the sake of this paper only

coordinates) plus formal errors and a standard goodness–of–fit parameter (a reduced chi–squared statistic).

3 CROSS-MATCH WITH PREVIOUS SURVEYS

We compiled a list of Pleiades member candidates published over the past decades by various groups (Table 1) to update their membership status with the photometry and astrometry in DR9 of the GCS (Table A1). This list will serve as starting point to identify new Pleiades members in the GCS data and derive the cluster luminosity and mass functions.

For the brightest members, we used the extensive compilation of 1417 sources from Stauffer et al. (2007) which includes candidate cluster members from several large-scale proper motion studies of the Pleiades (Trumpler 1921; Hertzsprung 1947; Artyukhina 1969; Jones 1981; Haro et al. 1982; van Leeuwen et al. 1986; Stauffer et al. 1991; Hambly et al. 1993; Pinfield et al. 2000; Adams et al. 2001; Deacon & Hambly 2004). We added candidates from a large number of additional papers dedicated to the Pleiades low-mass stars and brown dwarfs over the past 20 years, many sources being common to several studies which surveyed independently the same region of the cluster. The references are listed in Table 1 along with the original numbers of sources published by each study (All) and the corresponding numbers of candidates covered by the GCS (DR9). The success rate in the recovery of published candidate members is usually quite high (Table 1) because the GCS covers now the entire Pleiades cluster, as can be seen from Fig. 1. Earlier studies such as Hambly et al. (1993), Adams et al. (2001)[5], and the list of 916 high-probability member candidates from Deacon & Hambly (2004) are contained in Stauffer et al. (2007) fnd ocused not only on Pleiades very-low-mass stars but also on brighter members which are saturated on the UKIDSS images. Thus these higher mass members are not retrieved by our SQL query due to our photometric cuts at the bright end of the survey. Similarly, many L and T dwarf candidates reported by Bihain et al. (2006) and Casewell et al. (2007)[6] are too faint to be detected on the GCS images. Some of the earlier Pleiades candidates are not recovered mainly because (Table 1):

- 341 sources brighter than our saturation limits equivalent to 58.5% of previously published sources not recovered by our SQL query (mainly coming from early surveys as mentioned above)
- 185 sources (i.e. 31.7%) missing images in J, H, or $K1$
- 10 sources located in holes of the UKIDSS GCS coverage due to quality control issues (1.7% of all published members)
- 8 (or 1.37%) known Pleiades candidates located beyond our 3 arcsec cross-match limit, possibly because that they are higher proper motion non-members

To quantify the completeness limit of the GCS Pleiades dataset, we have listed in Column 1 of Table 1 (numbers in brackets) the numbers of previously-published candidates within the magnitude range probed by the GCS (see Section 2.1). The average of the percentages listed in the last column of Table 1 amounts for 92.2%, not taking into account the sample of Zapatero Osorio et al. (1997) due to problems with their coordinates. We also considered the most complete and updated sample of high-mass stars and low-mass Pleiades member candidates published by Stauffer et al. (2007). We recovered 94% of their sources, suggesting that overall our GCS sample is at least 92–94% complete.

Table A1 is provided in electronic format only with a total of 3196 known Pleiades member candidates reported in the literature. From this sample we removed the multiple detections and kept all different names from earlier studies in the last column for future searches: we are left with 1379 Pleiades candidates. We give the GCS DR9 coordinates of these 1379 Pleiades candidates, the $ZYJHK1K2$ photometry, the proper motions in right ascension and declination with their respective errors as well as the χ^2 value which represents the reduced chi-squared statistic of the astrometric fit for each source. This parameter is equal to the usual chi-squared statistic (sum of normalised residuals) divided by the degrees of freedom (i.e. number of data points minus the number of fitted parameters). The penultimate column supplies the membership probability for 1067 of the 1379 previously reported Pleiades candidates (see Section 4.1.1 for the method). A total of 312 out of 1379 Pleiades candidates have no membership probabilities because they are not classified as Pleiades members by the probabilistic selection (see Section 4.1 for the photometric and astrometric criteria). They are divided into four groups as follows: 190 sources detected in $ZYJHK$ but classified as proper motion non members, 42 objects without $Z+Y$ photometry, 74 objects without Z only, and 6 sources without Y only. The last column gives the old names used by earlier studies (names from different authors are separated by an underscore "_").

Previously-published Pleiades member candidates not recovered in the GCS DR9 are listed in Table B1 with their coordinates and old names from earlier studies. After removing common sources, we are left with 544 known Pleiades member candidates not in our sample. The large majority of these sources are either too bright or too faint to in the GCS database or photometric and/or astrometric non members of the Pleiades.

4 NEW SUBSTELLAR MEMBERS IN THE PLEIADES

4.1 Probabilistic approach

4.1.1 Method

In this section we outline the probabilistic approach we employed to select low-mass stars and brown dwarf member candidates of the Pleiades using photometry and astrometry from the UKIDSS GCS DR9. This method is described in detail in Deacon & Hambly (2004) and Lodieu et al. (2007). The main steps are:

(i) Define the cluster sequence using candidates published in the literature within the area covered by the latest release of the GCS

(ii) Make a conservative photometric cut in the ($Z-J$,Z) diagram to include known members and identify new cluster member candidates (dashed lines on the top-left panel in Fig. 6).

(iii) Analyse the vector point diagram in a probabilistic manner to assign a membership probability for each photometric candidate with a proper motion measurement (Section 4.1.2).

(iv) Obtain an illustrative list of high probability cluster members by choosing a specific threshold for the membership, chosen as p$\geqslant$0.6 here

(v) Derive the luminosity and mass function using all candidates with membership probabilities without any threshold for a complete count of the membership

[5] We should mention that this catalogue was not publish but is included in the Stauffer et al. (2007) compilation

[6] Four objects have wrong coordinates, rectified in the erratum of this paper (Casewell et al. 2010)

Table 1. Updated membership of Pleiades member candidates published in the literature and recovered by the GCS DR9. Papers dedicated to the Pleiades over the past two decades are ordered by year. References are: Hambly et al. (1993), Zapatero Osorio et al. (1997), Festin (1998), Bouvier et al. (1998), Zapatero Osorio et al. (1999), Hambly et al. (1999), Pinfield et al. (2000), Moraux et al. (2001), Jameson et al. (2002), Dobbie et al. (2002), Moraux et al. (2003), Deacon & Hambly (2004), Bihain et al. (2006), Lodieu et al. (2007), Casewell et al. (2007), and Stauffer et al. (2007). Columns 2 and 3 give the numbers of sources published by the reference given in Column 1 and the numbers of sources recovered in GCS DR9, respectively. Numbers in brackets in Column 1 represent all sources in a given catalogue within the magnitude range probed by the GCS. Columns 4 and 5 give the numbers of high-probability members (p$\geqslant$60%) and non members (NM) according to our probabilistic approach (first number) and method #2 (second number). The last column gives the percentages of sources recovered in the GCS DR9 (i.e. Column 2 divided by numbers in brackets in Column 1).

Survey	All	DR9	Memb	NM	%
Hambly1993	440 (440)	418	303/302	115/116	95.0
Zapatero1997a	9 (9)	2	1/1	1/1	22.2
Festin1998	45 (44)	37	24/24	13/13	84.1
Stauffer1998	20 (19)	16	11/10	5/6	84.2
Bouvier1998	26 (26)	25	12/15	13/10	96.2
Zapatero1999	46 (44)	38	8/13	30/25	86.4
Hambly1999	9 (9)	9	5/6	4/3	100.0
Pinfield2000	339 (338)	320	185/187	135/133	94.7
Moraux2001	25 (25)	25	12/15	13/10	100.0
Dobbie2002	90 (87)	61	8/9	53/52	70.0
Moraux2003	109 (108)	107	74/74	33/33	99.1
Deacon2004	916 (746)	674	467/450	207/224	90.3
Bihain2006	34 (31)	28	11/14	17/14	90.3
Lodieu2007	456 (456)	454	376/376	78/78	99.6
Casewell2007	23 (16)	16	4/7	9/6	100.0
Stauffer2007	1416 (944)	888	567/639	321/249	94.0

4.1.2 *Membership probabilities*

In order to calculate formal membership probabilities we used the same technique as Deacon & Hambly (2004) and Lodieu et al. (2007) to fit distribution functions to proper motion vector point diagrams (Hambly et al. 1995). We refer the reader to those papers for more details and additional equations. First we have rotated the vector point diagram so the cluster lies on the y-axis using the rotation transformation below (Equations 1 and 2):

$$\mu_{x1} = 0.03896 \times \mu_x - 0.921 \times \mu_y \quad (1)$$

$$\mu_{y1} = 0.03896 \times \mu_y - 0.921 \times \mu_x \quad (2)$$

corresponding a rotation angle of 23.7 degrees, assuming a relative proper motion of (19.7,−44.82) mas/yr for the Pleiades as measured on the vector point diagram created from the GCS DR9 data (slightly different from the Hipparcos absolute motion; van Leeuwen 2009). It is common to refer to the proper motions in the rotated vector point diagram as μ_{x1} and μ_{y1}.

We have assumed that there are two contributions to the total distribution $\phi(\mu_x, \mu_y)$, one from the cluster ($\phi_c(\mu_x, \mu_y)$) and one from the field stars ($\phi_f(\mu_x, \mu_y)$). The fitting region was delineated by $-50 < \mu_x < 50$ mas/yr and $20 < \mu_y < 70$ mas/yr. These were added by means of a field star fraction f to yield an expression for ϕ given in Equation 3:

$$\phi(\mu_x, \mu_y) = f\phi_f(\mu_x, \mu_y) + (1-f)\phi_c(\mu_x, \mu_y) \quad (3)$$

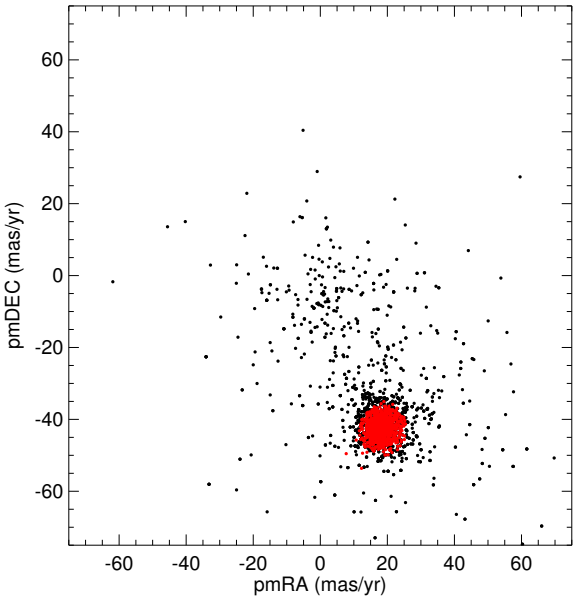

Figure 4. Vector point diagram showing the proper motion in right ascension (x-axis) and declination (y-axis) for previously-known member candidates recovered by the GCS DR9 (filled black dots) and the new member candidates with membership probabilities higher than 60% identified in this work (red dots).

We have assumed that the cluster distribution is characterised by a bivariate Gaussian with a single standard deviation σ and mean proper motion values in each axis μ_{xc} and μ_{yc} (Equation 4):

$$\phi_c \propto exp\left(-\frac{(\mu_x - \mu_{xc})^2 + (\mu_y - \mu_{yc})^2}{2\sigma^2}\right) \quad (4)$$

The field star distribution was fitted by a single Gaussian in the x axis (with standard deviation Σ_x and mean μ_{xf}) and a declining exponential in the y axis with a scale length τ. The use of a declining exponential is a standard method (e.g. Jones & Stauffer 1991) and is justified in that the field star distribution is not simply a circularly-symmetric error distribution (i.e. capable of being modelled as a 2d Gaussian) - rather there is a prefered direction of real field star motions resulting in a characteristic velocity ellipsoidal signature, i.e. a non-Gaussian tail, in the vector point diagram. This is best modelled (away from the central error-dominated distribution) as an exponential in the direction of the antapex (of the solar motion).

The best fitting set of parameters were chosen using a maximum likelihood method (see Deacon & Hambly 2004). However in a deviation from this method we did not fit for the standard deviation of the cluster proper motions (σ). Instead we calculated the mean astrometric error for all objects in each magnitude range and used this as our cluster standard deviation. This fitting process was tested by Deacon & Hambly (2004) where simulated data sets were created and run through the fitting process to recover the input parameters. These tests produced no significant offsets in the parameter values (see Table 3 and Appendix A of Deacon & Hambly 2004, for results and more details on the procedure). Hence, we have calculated the formal membership probabilities as,

$$p = \frac{\phi_c}{f\phi_f + (1-f)\phi_c} \quad (5)$$

Table 2. Summary of the results after running the programme to derive membership probabilities. For each Z magnitude range, we list the number of stars used in the fit (Nb), the field star fraction f, and parameters describing the cluster and field star distribution. Units are in mas/yr except for the number of stars and the field star fraction f. The cluster star distribution is described by the mean proper motions in the x and y directions (μ_{x_c} and μ_{y_c}) and a standard deviation σ. Similarly, the field star distribution is characterised by a scale length for the y axis (τ), a standard deviation Σ_x, and a mean proper motion in the x direction (μ_{x_f}).

Z	Nb	f	σ	μ_{x_c}	μ_{y_c}	τ	Σ_x	μ_{x_f}
12–13	486	0.86	3.22	-1.36	44.65	15.51	17.97	-9.48
13–14	853	0.79	3.14	0.21	46.25	14.95	17.46	-9.22
14–15	1394	0.78	3.21	-0.11	46.12	13.50	16.95	-9.13
15–16	1712	0.86	3.28	0.47	45.60	13.19	16.06	-9.45
16–17	1885	0.95	3.41	0.68	45.25	11.16	15.16	-9.79
17–18	1256	0.96	3.70	-0.26	44.99	9.58	14.28	-10.34
18–19	493	0.93	4.28	-1.23	44.07	11.02	15.09	-11.18
19–20	358	0.92	5.93	-0.63	45.76	10.30	15.72	-9.86
20–21	369	0.84	9.62	7.80	41.75	10.80	17.49	-7.76

As the astrometric errors are a function of magnitude we split the sample into nine bins. Each bin was one magnitude wide and the constituent stars used to fit for six of the seven parameters in the same way as described in Deacon & Hambly (2004). We used bins of one magnitude to have a sufficient number of Pleiades members in each range. In the faintest bins where the astrometric errors increase rapidly, the number of cluster stars was so small that we fixed the location of the cluster on the vector point diagram (μ_{xc} and μ_{yc}) to the values from a brighter bin. The other parameters were fitted as normal. A summary of the fitted parameters from the probabilistic analysis described above is given in Table 2.

Deacon & Hambly (2004) test the reliability of this method in Section 2.6 and find that the method accurately recovers the parameters from simulated datasets. We refer the reader to Table 3 in this paper for approximate errors on parameters but note that these tests were performed on simulated datasets with a much larger fraction of cluster stars. Hence our cluster parameters will likely have higher errors than those quoted. Some parameters such as τ and σ_x vary between magnitude bins due to noise as a result of two competing factors. As we go fainter the real proper motions of our field star contaminants decrease as our typical field star will be more distant but the measurement errors on the proper motions increase. Hence these two parameters which describe the proper motions of the field stars initially fall with increasing magnitude but as the measurement errors (as traced by the parameter σ) blow up, these in turn also increase.

4.1.3 Probabilistic sample

The probabilistic approach yielded a total sample of 8797 sources with membership probabilities assigned to each of them. This sample contains 947 sources with membership probabilities higher than 60% listed in Table C1. Relaxing the probability to 50% yields a sample of 1076 Pleiades member candidates. These high-probability members are displayed in Fig. 5 along with previously published Pleiades candidates.

We note that the sequence of member candidates in our probabilistic sample is very similar to the sequence of previously-known members down to Z = 16 mag (Fig. 5). However, we observe differences in the Z = 16–17 mag range and at fainter magnitudes, mainly because candidates identified in earlier surveys focusing on Pleiades brown dwarfs did not have as much as information as the GCS i.e. 6-band photometry and accurate astrometry down to ∼25 Jupiter masses. Hence, our new dataset allows us to reject many of the earlier substellar candidates either on photometric or astrometric grounds.

4.2 Photometry and proper motion selection

In this section we outline a more widely used method (referred to as method #2 in the rest of the paper) that we applied to select low-mass and substellar Pleiades member candidates. This procedure consists of selecting cluster candidates by applying stricter photometric cuts in various colour-magnitude diagrams supplemented by a proper motion selection (e.g. Lodieu et al. 2006, 2007). This method is complementary but independent from the probabilistic approach presented in the previous section.

First, we plotted several colour-magnitude diagrams (Fig. 5) to study the position of known Pleiades members identified in earlier studies and published over the past decades (Table 1). Based on these known members, we define a series of lines to select photometrically member candidates with photometry in $ZYJHK$ in four colour-magnitude diagrams as indicated below (dotted lines in the diagrams in Fig. 6):

- ($Z-J$,Z) = (0.50,12.0) to (1.05,17.0)
- ($Z-J$,Z) = (1.05,17.0) to (2.40,21.5)
- ($Z-K$,Z) = (1.20,11.5) to (1.95,17.0)
- ($Z-K$,Z) = (1.95,17.0) to (4.00,21.5)
- ($Y-J$,Y) = (0.30,11.5) to (0.55,16.5)
- ($Y-J$,Y) = (0.55,16.0) to (1.40,20.5)
- ($J-K$,J) = (0.70,11.0) to (0.70,16.5)
- ($J-K$,J) = (0.70,16.5) to (1.70,19.0)

These photometric cuts remain conservative and the contamination to the blue side of the Pleiades sequence is still high. Hence, the second step consisted of applying a proper motion selection in the vector point diagram (Fig. 4) to improve on the photometric selection. We applied a 3σ selection given the formal errors on the individual proper motions for each object, implying a completeness higher than 99% for normally–distributed errors. We assumed a mean proper motion of ($+18$, -42) mas/yr for the Pleiades, slightly different from the Hipparcos values (Robichon et al. 1999; van Leeuwen 2009) because the proper motion measurements are on a relative system rather than the Hipparcos system as described in Collins & Hambly (2012). The main advantage of this method is that it doesn't rely on a single radius for the proper motion selection but rather takes into account the increasing uncertainty on the proper motion measurements for fainter stars, and allows for different time baselines of the epoch frames affecting the proper motion errors.

After applying both the photometric and proper motion selections, we found a large number of objects lying to the blue of the Pleiades sequence. Hence, we applied an additional photometric cut in the ($Z-J$,Z) colour-magnitude diagram, eliminating all sources in the Z = 12–18 mag range and located to the left of a line defined by ($Z-J$,Z) = (0.6,12.0) to (1.2,16.5). This selection yielded a total 1147 low-mass stars and brown dwarfs with Z magnitude ranging from 12 to 21.5 (Table C1). This total number is similar to the number of high probability Pleiades member candidates identified via the probabilistic approach; we note however that the membership count from the different methods is identical

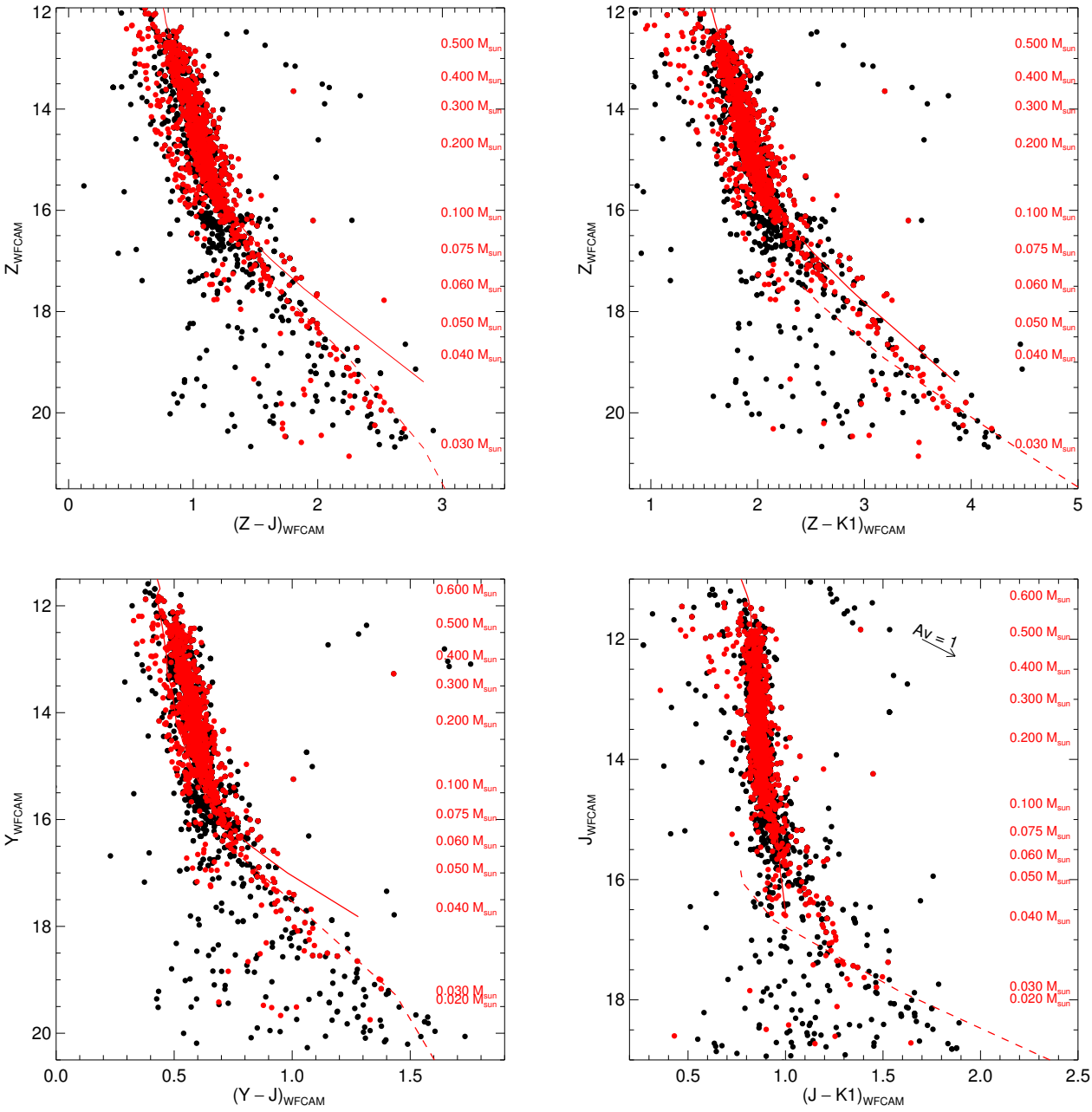

Figure 5. Colour-magnitude diagrams showing the Pleiades member candidates previously reported in the literature (black dots) and the new ones extracted from our probabilistic analysis (red dots). *Upper left:* $(Z-J,Z)$; *Upper right:* $(Z-K,Z)$; *Lower left:* $(Y-J,Y)$; *Lower right:* $(J-K,J)$. Overplotted are the 120 Myr NextGen (solid line; Baraffe et al. 1998) and DUSTY (dashed line; Chabrier et al. 2000) isochrones shifted to a distance of 120 pc. The mass scale is shown on the right hand side of the diagrams and spans ∼0.6–0.02 $M_{\odot}$, according to the 120 Myr isochrone models.

within the counting errors if we sum the membership probabilities of *all* stars, as expected.

4.3 Search for lower mass members

In this section we search for fainter and cool substellar members of the Pleiades by dropping the constraint on the Z-band detection and later the $Z+Y$ bands.

4.3.1 $YJHK$ detections

To extend the Pleiades cluster sequence to fainter brown dwarfs and cooler temperatures, we searched for potential candidate members undetected in Z. We imposed similar photometric and astrometric criteria as those detailed in Section 4.2 but imposed a Z non detection and associated criteria as described below:

- No Z detection
- $Y \geqslant 18$ and $J \leqslant 19.3$ mag

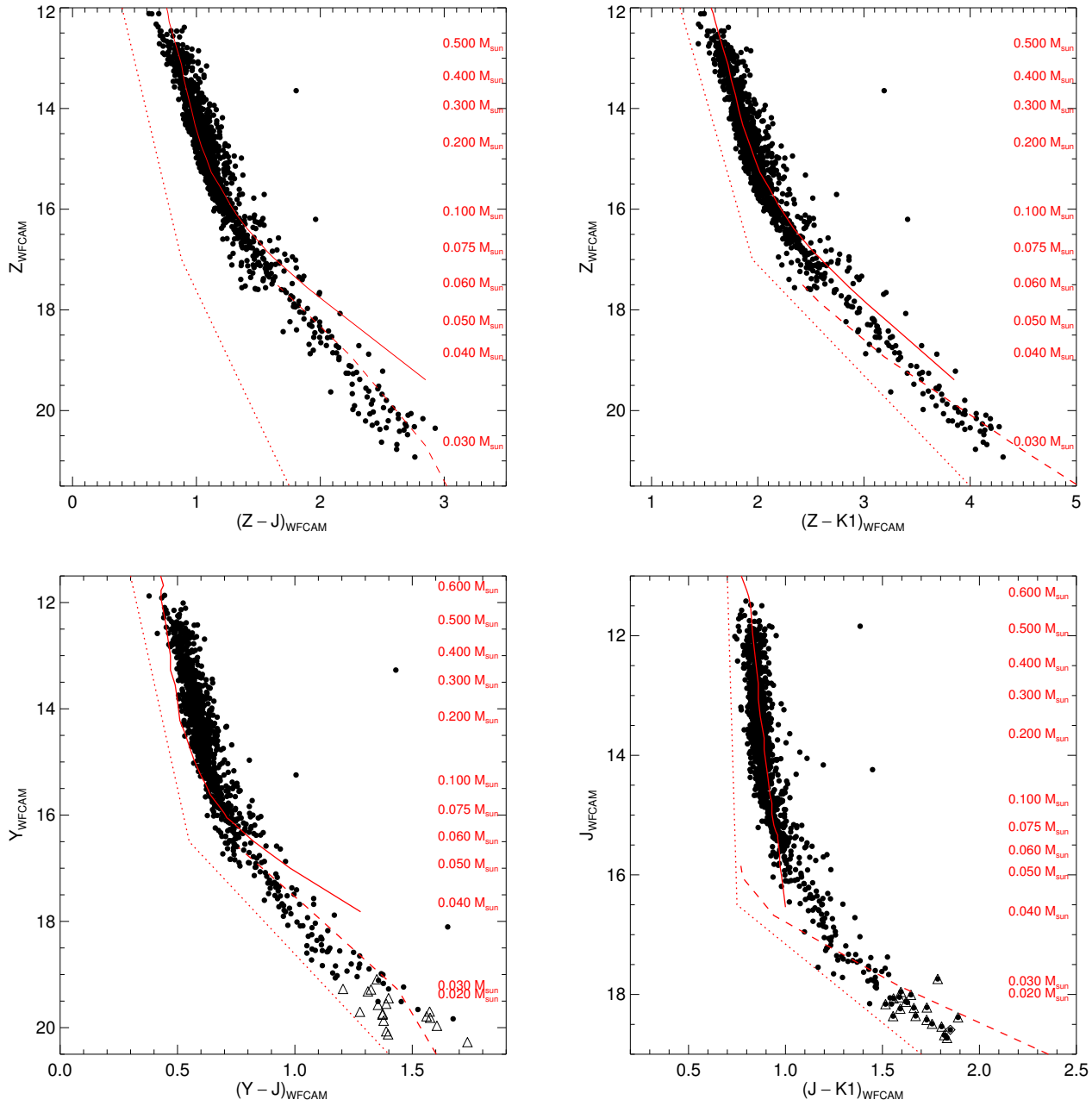

Figure 6. Same as Fig. 5 but only for Pleiades member candidates selected using method #2. The $YJHK$ and JHK-only detections have been added too. Our photometric criteria listed in Section 4.2 are represented by dotted lines. The faint $YJHK$ and JHK detections are highlighted with triangles and diamonds surrounding the black dots, respectively.

- Candidates should lie above the line defined by ($Y - J$,Y) = (0.55,16.0) and (1.40,20.5)
- Candidates should lie above the line defined by ($J - K$,J) = (0.75,16.5) and (1.70,19.0)
- The position on the proper motion vector point diagram of each candidate should not deviate from the assumed cluster proper motion by more than 3σ

This selection returned 22 additional Pleiades member candidates which have been added to Table C1 along with sources identified with both selection methods presented earlier. All but four of them are indeed invisible in the Z-band images and look well detected in the other bands after checking the GCS DR9 images by eye.

4.3.2 *JHK detections*

We repeated the procedure described above looking for Z and Y non detections. We applied the following criteria:

- No Z and Y detection
- J = 18–19.3 mag
- Candidates should lie above the line defined by ($J - K$,J) = (0.75,16.5) and (1.70,19.0)

• The position on the proper motion vector point diagram of each candidate should not deviate from the assumed cluster proper motion by more than 3σ

This query returned 19 new Pleiades candidate members. After checking the images by eye, we kept only one of them because one is actually visible in Y (although a Y detection is not reported in the GCS DR9 catalogue), one is visible in both the Z and Y images. The remaining 16 have no Z and Y images available so we can't confirm if they are indeed drop-outs (Table C1).

5 THE SUBSTELLAR BINARY FREQUENCY

The multiplicity in the substellar domain at different ages provides one way to constrain the formation mechanisms of brown dwarfs. As in our earlier study of the Pleiades (Lodieu et al. 2007), we investigated the binary frequency of Pleiades brown dwarfs using the photometry and colours from the GCS. However, our sample is now two times larger and, with the proper motions, is of much higher quality because it is drawn from the same homogeous survey. We consider in this section all Pleiades member candidates selected through method #2.

We applied the same method as described in Lodieu et al. (2007) to select substellar binary candidates in the Pleiades. We briefly summarise the technique here. Figure 7 displays two colour-magnitude diagrams used to identify binary candidates because of the large colour range and the presence of sources above the cluster (single star) sequence. We started off our selection in the ($Y - K1$,$K1$) colour-magnitude diagram (left-hand side plot in Fig. 7) because it shows large colour difference in the substellar regime. We applied the following method: for a given magnitude, e.g. $K1$ = 15.5–16.5 mag, we defined two horizontal lines intercepting the mean value of the single object sequence. From the intercept points we defined two vertical lines with a length of 0.75 mag (dashed lines in Fig. 7). Then we divided the box formed by both sequences and the vertical lines into two boxes: single stars lie in the bottom part whereas binary candidates in the top one. Except for one system which appears to the blue of the single-star sequence in the ($J - K1$,$K1$) diagram, the location of the binary candidates is confirmed in this diagram and others as well, adding credence to their potential multiplicity. Our method is corroborated by the presence of four known Pleiades brown dwarf binaries (IPMBD 25, IPMBD 29, PPl15, CFHT-Pl-IZ 4 Basri & Martín 1999; Martín et al. 2000, 2003; Bouy et al. 2006) above the single star sequence where Teide 1 (Rebolo et al. 1995), an isolated Pleiades brown dwarf is located (red symbol in Fig. 7). Note that we observe a dispersion of 0.5 mag in the single-star sequence which can explained by the tidal radius of the cluster leading to a variation of 10% in the distance of the members, i.e. $\sim$12 pc corresponding to $\sim$0.2 mag (Pinfield et al. 2000).

The binary fraction was then defined as the number of binaries divided by the total number of objects (single stars+binaries). We counted 51 binary candidates (Table D1) and 137 single stars in the $K1 \sim$ 14.32–16.27 mag range, corresponding to masses between 0.075 and 0.03 $M_{\odot}$ at the age and distance of the Pleiades. Hence, we derive a binary frequency of 51/(137+51) = 27.1$\pm$5.8% in this mass range for projected separations smaller than $\sim$100–200 au. This value is likely a lower limit because some binaries may hide in the single star sequence due to higher separations or mass ratios and we have not considered wider systems. The overall result is in agreement within the error bars with our previous estimate although on the lower side (36.5$\pm$8.0% Lodieu et al. 2007). We also divided up this mass range into two bins covering 0.075–0.05 $M_{\odot}$ and 0.05–0.03 $M_{\odot}$, yielding binary fractions of 33.0$\pm$9.1% (35 binaries and 71 singles) and 19.5$\pm$7.0% (16 binaries and 66 singles), respectively. The binary frequency over the lowest mass range is not reproduced by the latest hydrodynamical simulation of a 500 $M_{\odot}$ stellar cluster as no brown dwarf binary was found in the 0.07–0.03 $M_{\odot}$ range (Table 2 in Bate 2011). Unfortunately, we cannot test further those theoretical predictions with estimates on the numbers of triple and high-order multiple, separation distributions, and mass ratios.

We investigated the range of validity of our binary frequency by plotting the expected positions of binary systems with primary masses of 0.075, 0.05, and 0.03 $M_{\odot}$ (blue crosses in Fig. 7. Adding smaller mass brown dwarfs (going from 0.075 $M_{\odot}$ i.e. equal-mass binaries down to 0.02 $M_{\odot}$) to primaries with masses of 0.075 $M_{\odot}$ places those systems to the red of single stars and then turn over towards higher luminosities. The same behaviour is observed for binaries with primary masses of 0.05 $M_{\odot}$ whereas binaries with primary masses of 0.03 $M_{\odot}$ turn redder and brighter. To estimate the sensitivity of our binary frequency in terms of mass ratios, we considered the photometric errors of the GCS for the three mass values. We inferred that our binary frequencies over the 0.075–0.05 $M_{\odot}$ and 0.05–0.03 $M_{\odot}$ are valid for mass ratios larger than 0.4–0.5 and 0.8, respectively. Hence, the factor of two observed in the multiplicity between those two mass bins should be interpreted with caution because they are not valid over the same mass ratio interval. If we consider only binaries with mass ratios larger than 0.8 in the 0.075–0.05 $M_{\odot}$ mass range, we derive a binary fraction of 9/(71+9) = 11.3$\pm$5.0%, lower by a factor of two than the frequency inferred in the 0.05–0.03 $M_{\odot}$ range although consistent within the error bars.

We note that we applied the same procedure to the probabilistic sample and found very similar numbers which do not change the main conclusions discussed in this Section. We infer a substellar binary frequency of 24.3$\pm$7.3% which can be divided up into 29.2$\pm$12.0 and 20.0$\pm$8.7% for the 0.075–0.05 $M_{\odot}$ and 0.05–0.03 $M_{\odot}$ mass bins, respectively.

Our binary fraction is higher by a factor two to three than the frequency inferred from high-resolution imaging (13.3^{+13}_{-4}%; Martín et al. 2000, 2003; Bouy et al. 2006) especially if we consider that all known Pleiades brown dwarf binaries lie in the 0.065–0.055 $M_{\odot}$ mass range. Our multiplicity is lower than the 50% estimate derived by Pinfield et al. (2000) from a purely photometric estimate (i.e. no proper motion measurements involved) and on the low side of Monte-Carlo predictions (32–45%; Maxted & Jeffries 2005). However, our results are in agreement with the upper limit of 26$\pm$10% quoted by Basri & Reiners (2006) for low-mass stars and brown dwarfs. This total binary frequency is split into 11% of spectroscopic binaries with projected separation below 3 au, and 15% of wider binaries (3–15 au) in agreement with high-resolution imaging surveys of field ultracool dwarfs (for a review, see Burgasser et al. 2007) and theoretical predictions from hydrodynamical simulations (Bate 2011).

6 VARIABILITY AT 120 MYR

In this section we discuss the variability of the Pleiades low-mass stars and brown dwarfs using the two epochs provided by the GCS. We only considered the Pleiades member candidates with membership probabilities larger than 60%, many of them being already published in the literature (Tables A1 and C1).

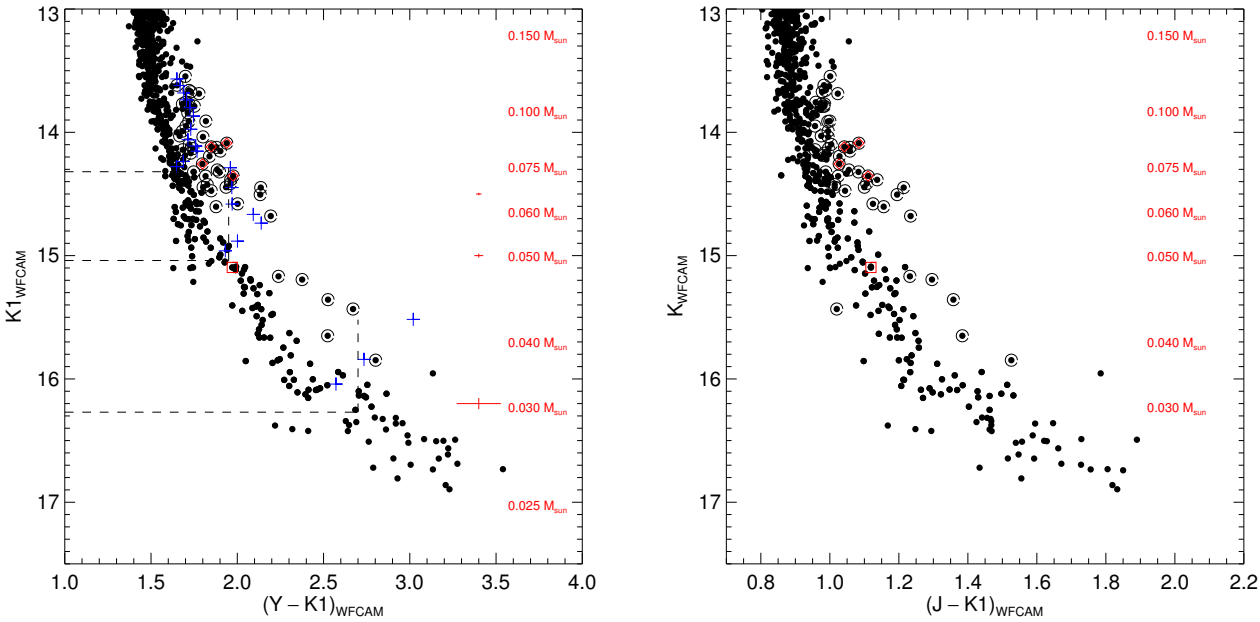

Figure 7. ($Y-K$,K) and ($J-K$,K) colour-magnitude diagrams showing all Pleiades member candidates selected with method #2 as well as the $YJHK$ and JHK-only detections. The multiple system candidates identified photometrically in the ($Y-K$,K) diagram are marked with a circle; the red square shows the location of the prototype Pleiades brown dwarf Teide 1. The mass scale is shown on the right hand side of the diagrams for an age of 120 Myr and a distance of 120.2 pc. Photometric error bars are shown as crosses on the right-hand side of the panel. The method describing the selection of binary candidates in the ($Y-K$,K) diagram is highlighted with black dashed lines. Blue crosses represent the expected sequences of binary systems for primaries with masses of 0.075, 0.05, and 0.03 M$_{\odot}$, respectively.

Figure 8 shows the ($K1$–$K2$) vs $K1$ for all Pleiades member candidates with probabilities higher than 60%. The brightening in the $K1$ = 11–12 mag range is due to the difference in saturation characteristics between the first and second epoch, of the order of 0.5 mag both in the saturation and completeness limit. This is understandable because the exposure times have been doubled for the second epoch with relaxed constraints on the seeing requirement and weather conditions. We excluded those objects from our variability study. Overall, the sequence indicates consistent photometry between the two K epochs and very few objects appear variable in the K-band.

We selected variable objects by looking at the standard deviation, defined as 1.48$\times$ the median absolute deviation which is the median of the sorted set of absolute values of deviation from the central value of the $K1$–$K2$ colour. In the $K1$ = 11–13 mag, we identified four potential variable abjects with differences in the K-band larger than 3σ above the standard deviation. However, all appeared saturated in the second epoch images suggesting that the variability may be caused by the inaccurate photometry derived from saturated sources. We extracted another potential variable low-mass star around K $\sim$14.5 mag but this source is located at the edge of the detector, casting doubt on any intrinsic variability. The analysis is not possible beyond 16 mag due to the small number of Pleiades members with high probabilities.

We conclude that the level of K–band variability at 120 Myr is small, with standard deviations in the 0.05–0.08 mag range, suggesting that it cannot account for the dispersion in the cluster sequence. The same conclusions are drawn from the sample derived from method #2.

7 THE INITIAL MASS FUNCTION

In this section we discuss the cluster luminosity and mass functions derived from the samples of Pleiades member candidates extracted from both methods described in the previous section. We did not attempt to correct the mass function for binaries.

7.1 The cluster luminosity function

In this section, we construct two luminosity functions: i) we used the sample of 8797 Pleiades cluster member candidates selected by the probabilistic approach (Section 4.1); and ii), the 1147 candidates identified with method #2 (Section 4.2). The luminosity function of the former method is derived by summing membership probabilities of all stars fitted to distribution functions in the vector point diagram, whereas the luminosity function of the latter is derived simply by summing the number of member candidates.

Both luminosity functions i.e. the number of stars and brown dwarfs as a function of magnitude plotted per 0.5 mag bin is displayed in Fig. 9. The brightest bin is a lower limit due to the saturation limit of the GCS survey. The last bin is very likely incomplete due to the constraint imposed on the Z-band detection. The numbers of objects per 0.5 mag bin increase quickly to reach a peak around Z = 14.5–15 and drop off afterwards down to the completeness of our survey with a possible peak beyond Z = 20 mag (Tables 3 & 4). Both luminosity functions look very similar and match each other within the error bars. Therefore, we conclude that both methods provide the same result and a good representation of the Pleiades luminosity and mass functions.

Assuming that the observed lithium depletion boundary is at M $\sim$ 0.075 M$_{\odot}$ (M$_Z$ = 11.44 Stauffer et al. 1998; Barrado y

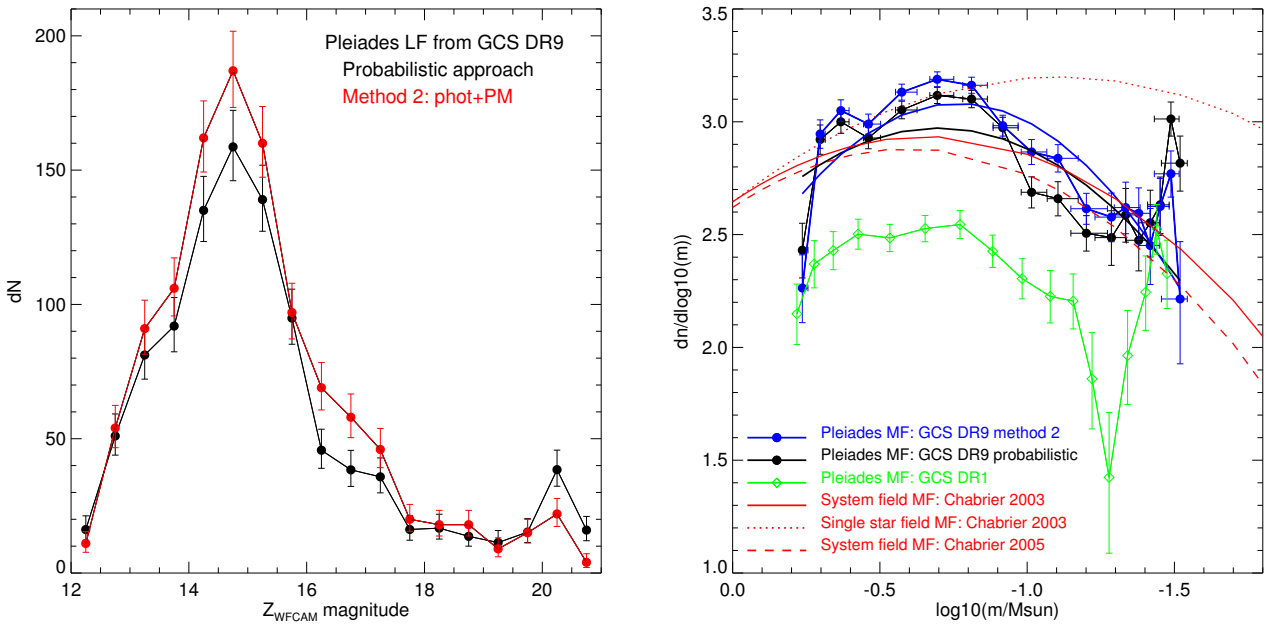

Figure 9. Luminosity (left) and mass (right) functions derived from our analysis of the UKIDSS GCS DR9 sample of Pleiades member candidates. The left-hand side panel compares the luminosity function obtained from the probabilistic approach (black symbols and black line) and the luminosity function derived from the selection outlined by method #2 (red colour). Error bars on the number of objects per magnitude bin are Gehrels errors. The right-hand side panel compares the Pleiades mass function derived from the probabilistic approach (filled black dots linked by a solid line) and the mass function derived from method #2 (blue symbols and blue line). The black and blue lines are log-normal fits to the Pleiades mass function. Error bars on the dN/dlogM are Gehrels errors whereas error bars on the masses come from the 3σ lower and upper limits on the age (100–150 Myr) and distance (114.5–125.9 pc). The first and last two points of the Pleiades luminosity and mass functions are to be treated with caution due to saturation and contamination at the bright and faint ends, respectively. The mass function from our GCS DR1 analysis (green diamond and green line) and the field mass functions (red lines; Chabrier 2003, 2005) are also included for completeness and comparison.

Table 3. Values for the luminosity and mass functions (both in linear and logarithmic scales) per magnitude and mass bin for the Pleiades open cluster using the probabilistic approach (method 1). We assume a distance of 120.2 pc and employed the NextGen and DUSTY 120 Myr theoretical isochrones for the mean values. The uncertainties given in brackets for the mid-mass (Column 4) come from the 3σ lower and upper limits on the age and distance, assuming errors of 8 Myr and 1.9 pc, respectively.

Mag range	Nb_obj	Mass range	Mid-mass	dN	errH	errL	dn/dM	errH	errL	dN/dlogM	errH	errL
12.0–12.5	179	0.6200–0.5400	0.5800 (0.5550–0.5890)	16.18	5.11	3.99	202.29	63.94	49.90	2.43	0.27	0.28
12.5–13.0	306	0.5400–0.4690	0.5045 (0.4850–0.5125)	51.03	8.20	7.13	718.70	115.43	100.36	2.92	0.15	0.15
13.0–13.5	372	0.4690–0.3890	0.4290 (0.4025–0.4380)	81.18	10.05	9.00	1014.71	125.64	112.45	3.00	0.12	0.12
13.5–14.0	480	0.3890–0.3030	0.3460 (0.3145–0.3595)	91.95	10.63	9.58	1069.15	123.58	111.35	2.93	0.11	0.11
14.0–14.5	614	0.3030–0.2300	0.2665 (0.2365–0.2800)	135.02	12.65	11.61	1849.55	173.31	159.03	3.05	0.09	0.09
14.5–15.0	779	0.2300–0.1740	0.2020 (0.1775–0.2140)	158.64	13.63	12.59	2832.91	243.31	224.74	3.12	0.08	0.08
15.0–15.5	848	0.1740–0.1350	0.1545 (0.1365–0.1655)	139.02	12.82	11.78	3564.67	328.78	302.06	3.10	0.09	0.09
15.5–16.0	863	0.1350–0.1070	0.1210 (0.1073–0.1305)	94.90	10.78	9.73	3389.36	385.01	347.46	2.97	0.11	0.11
16.0–16.5	931	0.1070–0.0862	0.0966 (0.0858–0.1048)	45.73	7.82	6.74	2198.46	375.84	324.22	2.69	0.16	0.16
16.5–17.0	953	0.0862–0.0710	0.0786 (0.0671–0.0855)	38.41	7.26	6.18	2527.30	477.51	406.43	2.66	0.17	0.18
17.0–17.5	747	0.0710–0.0549	0.0630 (0.0534–0.0711)	35.81	7.05	5.96	2224.41	437.69	370.40	2.51	0.18	0.18
17.5–18.0	508	0.0549–0.0486	0.0517 (0.0463–0.0589)	16.22	5.12	4.00	2574.60	812.61	634.33	2.49	0.27	0.28
18.0–18.5	268	0.0486–0.0440	0.0463 (0.0414–0.0506)	16.70	5.18	4.06	3630.65	1125.53	881.74	2.59	0.27	0.28
18.5–19.0	224	0.0440–0.0396	0.0418 (0.0383–0.0461)	13.66	4.80	3.66	3105.68	1090.16	832.42	2.47	0.30	0.31
19.0–19.5	164	0.0396–0.0368	0.0382 (0.0356–0.0420)	11.34	4.48	3.33	4051.07	1599.11	1189.51	2.55	0.33	0.35
19.5–20.0	193	0.0368–0.0339	0.0353 (0.0330–0.0390)	15.26	5.00	3.87	5260.69	1724.40	1335.78	2.63	0.28	0.29
20.0–20.5	223	0.0339–0.0311	0.0325 (0.0305–0.0370)	38.49	7.26	6.18	13745.71	2594.29	2208.46	3.01	0.17	0.18
20.5–21.0	145	0.0311–0.0294	0.0302 (0.0286–0.0350)	15.99	5.09	3.97	9408.24	2995.26	2334.04	2.82	0.28	0.29

Table 4. Same as Table 3 but for method #2.

Mag range	Nb_obj	Mass range	Mid-mass	dN	errH	errL	dN/dM	errH	errL	dN/dlogM	errH	errL
12.0–12.5	11	0.6200–0.5400	0.5800 (0.5550–0.5890)	11.00	4.43	3.28	137.50	55.35	40.98	2.26	0.34	0.35
12.5–13.0	54	0.5400–0.4690	0.5045 (0.4850–0.5125)	54.00	8.40	7.33	760.56	118.30	103.26	2.95	0.14	0.15
13.0–13.5	91	0.4690–0.3890	0.4290 (0.4025–0.4380)	91.00	10.58	9.53	1137.50	132.23	119.08	3.05	0.11	0.11
13.5–13.0	106	0.3890–0.3030	0.3460 (0.3145–0.3595)	106.00	11.33	10.28	1232.56	131.77	119.58	2.99	0.10	0.10
14.0–14.5	162	0.3030–0.2300	0.2665 (0.2365–0.2800)	162.00	13.76	12.72	2219.18	188.46	174.22	3.13	0.08	0.08
14.5–15.0	187	0.2300–0.1740	0.2020 (0.1775–0.2140)	187.00	14.70	13.67	3339.29	262.54	244.03	3.19	0.08	0.08
15.0–15.5	160	0.1740–0.1350	0.1545 (0.1365–0.1655)	160.00	13.68	12.64	4102.56	350.74	324.08	3.16	0.08	0.08
15.5–16.0	97	0.1350–0.1070	0.1210 (0.1073–0.1305)	97.00	10.89	9.84	3464.29	388.82	351.29	2.98	0.11	0.11
16.0–16.5	69	0.1070–0.0862	0.0966 (0.0858–0.1048)	69.00	9.35	8.29	3317.31	449.60	398.63	2.87	0.13	0.13
16.5–17.0	58	0.0862–0.0710	0.0786 (0.0671–0.0855)	58.00	8.66	7.60	3815.79	570.06	499.96	2.84	0.14	0.14
17.0–17.5	46	0.0710–0.0549	0.0630 (0.0534–0.0711)	46.00	7.84	6.76	2857.14	486.79	420.12	2.61	0.16	0.16
17.5–18.0	20	0.0549–0.0486	0.0517 (0.0463–0.0589)	20.00	5.56	4.44	3174.60	881.78	705.41	2.58	0.25	0.25
18.0–18.5	18	0.0486–0.0440	0.0463 (0.0414–0.0506)	18.00	5.33	4.21	3913.04	1158.72	915.89	2.62	0.26	0.27
18.5–19.0	18	0.0440–0.0396	0.0418 (0.0383–0.0461)	18.00	5.33	4.21	4090.91	1211.39	957.52	2.59	0.26	0.27
19.0–19.5	9	0.0396–0.0368	0.0382 (0.0356–0.0420)	9.00	4.12	2.96	3214.29	1472.32	1056.44	2.45	0.38	0.40
19.5–20.0	15	0.0368–0.0339	0.0353 (0.0330–0.0390)	15.00	4.97	3.84	5172.41	1713.32	1324.34	2.62	0.29	0.30
20.0–20.5	22	0.0339–0.0311	0.0325 (0.0305–0.0370)	22.00	5.77	4.66	7857.14	2060.61	1665.60	2.77	0.23	0.24
20.5–21.0	4	0.0311–0.0294	0.0302 (0.0286–0.0350)	4.00	3.18	1.94	2352.94	1870.26	1139.11	2.21	0.58	0.66

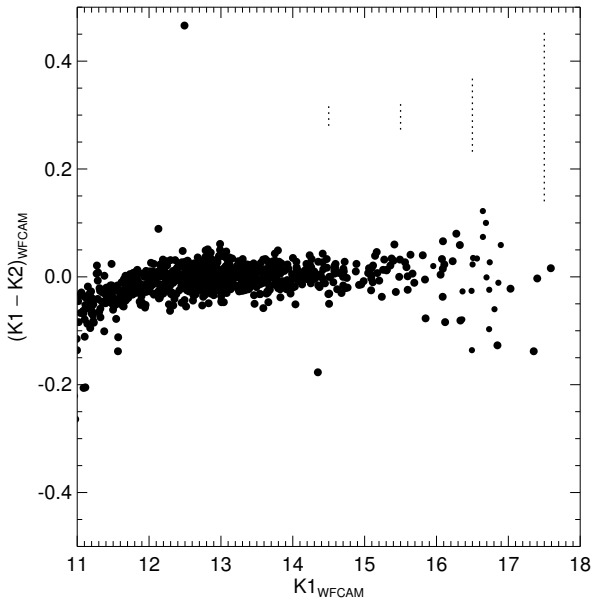

Figure 8. Difference in the K magnitude ($K1$–$K2$) as a function of the $K1$ magnitude for all Pleiades member candidates with membership probability greater than 60%. The $YJHK$ and JHK-only detections have been added too. Typical error bars on the colour shown as vertical dotted lines are added at the top of the plot.

Navascués et al. 2004) and a distance of 120.2 pc, the sample extracted by method #2 contains 1147 Pleiades member candidates, divided up into 978 stars (83.3%) and 169 brown dwarfs (14.7%). Similar percentages are obtained considering the sample of 947 high probability members (p$\geqslant$60%) identified in the probabilistic approach with 10.3% of brown dwarfs. Hence, the star ($\sim$0.6–0.08 $M_{\odot}$) to brown dwarf (0.08–0.03 $M_{\odot}$) ratio in the Pleiades lies between 5.4–6.3 and 8.6–9.3 if we consider a 3σ limit in the distance of the Pleiades (114.5–125.9 pc; van Leeuwen 2009). These numbers are in agreement with measurements (with slightly different mass ranges depending on the survey) derived from the field mass function (1.7–5.3; Kroupa 2002; Chabrier 2005; Andersen et al. 2006), young star-forming regions (3.0–6.4 for the Trapezium Cluster; 3.8-4.3 for σ Orionis; 3.8 for Chamaeleon; 8.3–11.6 for IC 348; Hillenbrand & Carpenter 2000; Muench et al. 2002; Luhman et al. 2003; Andersen et al. 2006; Luhman 2007; Lodieu et al. 2009), open clusters (3.7 for the Pleiades and 4.5 for M35; Bouvier et al. 1998; Barrado y Navascués et al. 2001), and hydrodynamical simulations of star clusters (3.8–5.0; Bate 2009, 2011).

7.2 The cluster mass function

In this section we adopt the logarithmic form of the Initial Mass Function as originally proposed by Salpeter (1955): $\xi(\log_{10} m)$ = dn/d$\log_{10}(m) \propto$ m$^{-\alpha}$. We converted the luminosity into a mass function using the NextGen models (Baraffe et al. 1998) for stars and brown dwarfs more massive than 50 $M_{\rm Jup}$ ($T_{\rm eff}$) and the DUSTY models (Chabrier et al. 2000) for less massive brown dwarfs. The Z = 12–21.5 mag range translates into masses between 0.62 and 0.03 $M_{\odot}$, assuming a revised distance of 120.2 pc (van Leeuwen 2009) and an age of 120 Myr for which the models are computed.

We included in Fig. 9 errors in both the x-axis (logM) and y-axis (dN/dlogM) as follows. For the error bars on the masses, we considered three times the uncertainties on the age (125$\pm$8 Myr; Stauffer et al. 1998) and distance (120.2$\pm$1.9 pc; van Leeuwen 2009) of the Pleiades given us a validity range of 3σ on the x-axis. Hence, we computed the masses with the 100 Myr NextGen and DUSTY isochrones shifted at a distance of 114.5 pc to define the lower limit and repeated the procedure with the 150 Myr isochrones for a distance of 125.9 pc as upper limits. (The uncertainties on the y-axis i.e. the dN/dlogM values are simply Gehrels error bars). The highest-mass point is incomplete due to the saturation of the GCS as are the two lowest-mass points of the mass function because the last two magnitude bins in the Z-band are more contaminated. Using these upper and lower bounds for the predicted masses for cluster members we refit the log–normal MF to examine the effects on the parameters of the fit (Fig. 10.) Following the Chabrier (2003) Gaussian parameterisation (his Equation 12) we find a characteristic mass $m_c = 0.24^{+0.01}_{-0.03}$ $M_{\odot}$ and a mass disper-

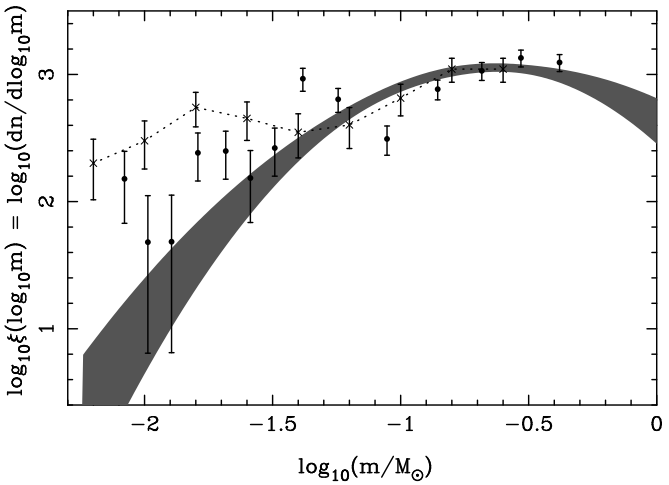

Figure 10. Mass function comparison between the Pleiades (shaded region showing a 1σ confidence interval from a weighted least–squares log–normal fit to the data presented here and extrapolated to lower masses) along with data from σ Orionis (filled circles; Lodieu et al. 2009) and Upper Sco (crosses joined by a dashed line; Lodieu et al. 2011). These have been normalised at the peak of the MF.

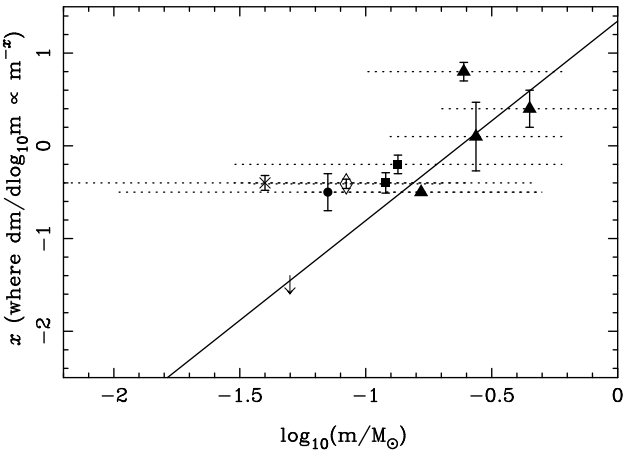

Figure 11. 'x-plot' equivalent to the 'Alpha plot' (where $x = \alpha - 1$, cf. Chabrier (2005)) showing the gradient of the mass function as a function of mass. The straight line is the gradient of the log–normal fit to the Pleiades data presented herein, while the filled circle is the recent GCS results from σ Orionis (α=0.5$\pm$0.2; Lodieu et al. 2009), the cross is from a power-law fit to the most recent Upper Sco results ($x = -0.6 \pm 0.08$; Lodieu et al. 2011), the open diamond for Alpha Per (α=0.59$\pm$0.05) from Barrado y Navascués et al. (2002), and the filled triangles are the results from Praesepe (α=1.4$\pm$0.2; α=1.8$\pm$0.1; α=1.11$\pm$0.37; Kraus & Hillenbrand 2007; Boudreault et al. 2010; Baker et al. 2010). The arrow indicates the upper limit to the mass function of the field brown dwarf population (Burningham et al. 2010). Horizontal dotted lines indicate mass ranges for power–law IMF determinations.

sion $\sigma = 0.44 \pm 0.01$ (Chabrier (2005) quotes $m_c = 0.25$ and $\sigma = 0.55$ for the disk system MF whereas Chabrier (2003) quotes $m_c = 0.22$ and $\sigma = 0.57$).

Overall we find that our Pleiades mass function is well represented by a log-normal form over the 0.6–0.03 $M_\odot$ mass range with a characteristic mass of 0.24 $M_\odot$ (Fig. 10). This result is in agreement with all previous studies in the Pleiades (Moraux et al. 2001; Tej et al. 2002; Dobbie et al. 2002; Deacon & Hambly 2004) over the same mass range and consistent with the extrapolation of the system field mass function (Chabrier 2005) which can also reproduce preliminary densities of field L and T dwarfs found in large-scale surveys (Metchev et al. 2008; Burningham et al. 2010; Reylé et al. 2010; Kirkpatrick et al. 2011) as displayed in Fig. 9. All these determinations of the mass function support the universality of the IMF as discussed in the review of Bastian et al. (2010) except for the case of Taurus (Briceño et al. 2002; Luhman et al. 2003). The latest hydrodynamical simulation of Bate (2011) is able to reproduce the observed field mass function (Kroupa 2002; Chabrier 2005) with high confidence after inclusion of radiative feedback, in agreement with independent calculations (Offner et al. 2009; Urban et al. 2010; Krumholz et al. 2011).

It is interesting to compare an extrapolation to lower masses of the log–normal Pleiades mass function derived here with results from other younger GCS targets (Fig. 10). While the Pleiades is measured in a higher mass range and shows a closely log–normal form, the IMF from a carefully cleaned spectroscopic sample in Upper Sco (Lodieu et al. 2011) penetrates to lower masses and seems to be much shallower in the substellar regime, implying the presence of more brown dwarfs. Results for the sigma Orionis cluster show a similar trend (Lodieu et al. 2009), although to a less obvious extent. Of course, these mass functions have been derived assuming that the evolutionary models accurately predict colours, bolometric magnitudes and temperatures at the different ages (especially ages < 10 Myr) and assuming also that any systematic errors introduced by not accounting for unresolved binarity cancel in the comparison. In Fig. 11 we show an 'x-plot' equivalent to the 'alpha plot' with $x = \alpha - 1$), i.e. a plot of the gradient of mass function as a function of mass, in order to compare with the constraints set on the field IMF gradient by the UKIDSS Large Area Survey T–type brown dwarf searches (e.g. Lodieu et al. 2007; Pinfield et al. 2008; Burningham et al. 2010)). While the mass functions of the more aged populations like Praesepe (Kraus & Hillenbrand 2007; Boudreault et al. 2010; Baker et al. 2010) or the field (Metchev et al. 2008; Burningham et al. 2010; Reylé et al. 2010; Kirkpatrick et al. 2011) show gradients consistent with the Pleiades log–normal, power–law fits to the very young Upper Sco ($x = -0.4 \pm 0.08$; Lodieu et al. 2011) and σ Orionis (x=-0.5$\pm$0.2; Lodieu et al. 2009) clusters are flatter. This may be evidence of a variation in the substellar IMF, or simply an artefact of systematic errors in the evolutionary model predictions at very young ages or age spreads. We should emphasise that the upper limit set for the field mass function by Burningham et al. (2010) remains under debate (due to the lack of constraints on masses and ages) as the CFHT brown dwarf survey (Reylé et al. 2010) and the preliminary densities determined by WISE (Kirkpatrick et al. 2011) suggest positive α values for the mass function in the T dwarf regime (see also Metchev et al. 2008).

8 SUMMARY

We have presented the outcome of a wide ($\sim$80 square degrees) and deep ($J \sim 18.8$ mag) survey in the Pleiades open cluster as part of the UKIDSS Galactic Clusters Survey Data Release 9. The main results of our analysis can be summarised as follows:

- we recovered Pleiades member candidates previously published and updated their membership assignations
- we selected photometrically and astrometrically potential Pleiades member candidates using two independent but complementary methods: the probabilistic analysis and a more standard method combining photometry and proper motion cuts

• we derived a BD binary fraction around 25.6±4.5% in the 0.075–0.03 $M_{\odot}$ mass range with a difference of a factor of two between high-mass (0.075–0.05 $M_{\odot}$) and low-mass (0.05–0.03 $M_{\odot}$) brown dwarfs for separations less than ∼100–200 au

• we investigated the K-band variability of Pleiades members and found virtually no variability at the level of 0.08 mag

• we derived the luminosity function from both selection methods and found no difference within the error bars

• we derived the Pleiades mass function which is best fit by a log-normal function peaking at 0.16–0.20 $M_{\odot}$ in the 0.6–0.03 $M_{\odot}$ range, in agreement with previous studies in the cluster and the extrapolation of the system field mass function

This paper represents a significant improvement in our knowledge of the Pleiades population and the cluster mass function in the substellar regime over the full cluster. We believe that this paper will represent a reference for many more years to come. We will now extend this study to other regions surveyed by the GCS to adress the question of the universality of the mass function using an homogeneous set of photometric and astrometric data. Future work to constraint current models of star formation include the search for companions to investigate their multiplicity properties, the determination of the radial velocities of Pleiades members, and deeper surveys to test the theory of the fragmentation limit.

ACKNOWLEDGMENTS

NL is funded by the Ramón y Cajal fellowship number 08-303-01-02 and the national program AYA2010-19136 funded by the Spanish ministry of science and innovation. This work is based in part on data obtained as part of the UKIRT Infrared Deep Sky Survey (UKIDSS). The UKIDSS project is defined in Lawrence et al. (2007). UKIDSS uses the UKIRT Wide Field Camera (WFCAM; Casali et al. 2007). The photometric system is described in Hewett et al. (2006), and the calibration is described in Hodgkin et al. (2009). The pipeline processing and science archive are described in Irwin et al. (in prep) and Hambly et al. (2008), respectively. We thank our colleagues at the UK Astronomy Technology Centre, the Joint Astronomy Centre in Hawaii, the Cambridge Astronomical Survey and Edinburgh Wide Field Astronomy Units for building and operating WFCAM and its associated data flow system. We are grateful to Isabelle Baraffe and France Allard for providing us with the NextGen, DUSTY and COND models for the WFCAM filters.

This research has made use of the Simbad database, operated at the Centre de Données Astronomiques de Strasbourg (CDS), and of NASA's Astrophysics Data System Bibliographic Services (ADS). This publication has also made use of data products from the Two Micron All Sky Survey, which is a joint project of the University of Massachusetts and the Infrared Processing and Analysis Center/California Institute of Technology, funded by the National Aeronautics and Space Administration and the National Science Foundation.

REFERENCES

Adams J. D., Stauffer J. R., Monet D. G., Skrutskie M. F., Beichman C. A., 2001, AJ, 121, 2053
Andersen M., Meyer M. R., Oppenheimer B., Dougados C., Carpenter J., 2006, AJ, 132, 2296
Artyukhina N. M., 1969, 12, 987
Baker D. E. A., Jameson R. F., Casewell S. L., Deacon N., Lodieu N., Hambly N., 2010, MNRAS, 408, 2457
Baraffe I., Chabrier G., Allard F., Hauschildt P. H., 1998, A&A, 337, 403
Barrado y Navascués D., Stauffer J. R., Jayawardhana R., 2004, ApJ, 614, 386
Barrado y Navascués D., Bouvier J., Stauffer J. R., Lodieu N., McCaughrean M. J., 2002, A&A, 395, 813
Barrado y Navascués D., Stauffer J. R., Bouvier J., Martín E. L., 2001, ApJ, 546, 1006
Basri G., Martín E. L., 1999, AJ, 118, 2460
Basri G., Reiners A., 2006, AJ, 132, 663
Bastian N., Covey K. R., Meyer M. R., 2010, ArXiv e-prints
Bate M. R., 2009, MNRAS, 392, 590
Bate M. R., 2011, MNRAS, 418, 703
Béjar V. J. S., et al. 2001, ApJ, 556, 830
Bihain G., Rebolo R., Béjar V. J. S., Caballero J. A., Bailer-Jones C. A. L., Mundt R., Acosta-Pulido J. A., Manchado Torres A., 2006, A&A, 458, 805
Bihain G., Rebolo R., Zapatero Osorio M. R., Béjar V. J. S., Caballero J. A., 2010, A&A, 519, A93
Boudreault S., Bailer-Jones C. A. L., Goldman B., Henning T., Caballero J. A., 2010, A&A, 510, A27+
Bouvier J., Stauffer J. R., Martín E. L., Barrado y Navascués D., Wallace B., Béjar V. J. S., 1998, A&A, 336, 490
Bouy H., Moraux E., Bouvier J., Brandner W., Martín E. L., Allard F., Baraffe I., Fernández M., 2006, ApJ, 637, 1056
Briceño C., Luhman K. L., Hartmann L., Stauffer J. R., Kirkpatrick J. D., 2002, ApJ, 580, 317
Burgasser A. J., et al. eds, Protostars and Planets V Not Alone: Tracing the Origins of Very-Low-Mass Stars and Brown Dwarfs Through Multiplicity Studies. pp 427–441
Burningham B., et al. 2010, MNRAS, 406, 1885
Casali M., et al. 2007, A&A, 467, 777
Casewell S. L., Dobbie P. D., Hodgkin S. T., Moraux E., Jameson R. F., Hambly N. C., Irwin J., Lodieu N., 2007, MNRAS, 378, 1131
Casewell S. L., Dobbie P. D., Hodgkin S. T., Moraux E., Jameson R. F., Hambly N. C., Irwin J., Lodieu N., 2010, MNRAS, 402, 1407
Casewell S. L., Jameson R. F., Burleigh M. R., Dobbie P. D., Roy M., Hodgkin S. T., Moraux E., 2011, MNRAS, 412, 2071
Chabrier G., 2003, PASP, 115, 763
Chabrier G., 2005, in E. Corbelli, F. Palla, & H. Zinnecker ed., The Initial Mass Function 50 Years Later Vol. 327 of Astrophysics and Space Science Library, The Initial Mass Function: from Salpeter 1955 to 2005. p. 41
Chabrier G., Baraffe I., Allard F., Hauschildt P., 2000, ApJ, 542, 464
Cutri R. M., et al. 2003, 2MASS All Sky Catalog of point sources, 2246
Deacon N. R., Hambly N. C., 2004, A&A, 416, 125
Dobbie P. D., Kenyon F., Jameson R. F., Hodgkin S. T., Pinfield D. J., Osborne S. L., 2002, MNRAS, 335, 687
Dobbie P. D., Pinfield D. J., Jameson R. F., Hodgkin S. T., 2002, MNRAS, 335, L79
Festin L., 1998, A&A, 333, 497
Gatewood G., de Jonge J. K., Han I., 2000, ApJ, 533, 938
Hambly N. C., et al. 2008, MNRAS, 384, 637
Hambly N. C., Hawkins M. R. S., Jameson R. F., 1993, A&AS, 100, 607

Hambly N. C., Hodgkin S. T., Cossburn M. R., Jameson R. F., 1999, MNRAS, 303, 835
Hambly N. C., Steele I. A., Hawkins M. R. S., Jameson R. F., 1995, MNRAS, 273, 505
Haro G., Chavira E., Gonzalez G., 1982, Boletin del Instituto de Tonantzintla, 3, 3
Hertzsprung E., 1947, Annalen van de Sterrewacht te Leiden, 19, A1
Hewett P. C., Warren S. J., Leggett S. K., Hodgkin S. T., 2006, MNRAS, 367, 454
Hillenbrand L. A., Carpenter J. M., 2000, ApJ, 540, 236
Hodgkin S. T., Irwin M. J., Hewett P. C., Warren S. J., 2009, MNRAS, 394, 675
Jameson R. F., Dobbie P. D., Hodgkin S. T., Pinfield D. J., 2002, MNRAS, 335, 853
Jameson R. F., Skillen I., 1989, MNRAS, 239, 247
Johnson H. L., 1957, ApJ, 126, 121
Jones B. F., 1981, AJ, 86, 290
Jones B. F., Stauffer J. R., 1991, AJ, 102, 1080
Kirkpatrick J. D., et al. 2011, ApJS, 197, 17
Kraus A. L., Hillenbrand L. A., 2007, AJ, 134, 2340
Kroupa P., 2002, Science, 295, 82
Krumholz M. R., Klein R. I., McKee C. F., 2011, ApJ, 740, 74
Lawrence A., et al. 2007, MNRAS, 379, 1599
Lodieu N., Dobbie P. D., Deacon N. R., Hodgkin S. T., Hambly N. C., Jameson R. F., 2007, MNRAS, 380, 712
Lodieu N., et al. 2007, MNRAS, 379, 1423
Lodieu N., Dobbie P. D., Hambly N. C., 2011, A&A, 527, A24
Lodieu N., Hambly N. C., Jameson R. F., 2006, MNRAS, 373, 95
Lodieu N., Hambly N. C., Jameson R. F., Hodgkin S. T., Carraro G., Kendall T. R., 2007, MNRAS, 374, 372
Lodieu N., Zapatero Osorio M. R., Rebolo R., Martín E. L., Hambly N. C., 2009, A&A, 505, 1115
Lucas P. W., Roche P. F., 2000, MNRAS, 314, 858
Luhman K. L., 1999, ApJ, 525, 466
Luhman K. L., 2007, ApJS, 173, 104
Luhman K. L., Briceño C., Stauffer J. R., Hartmann L., Barrado y Navascués D., Caldwell N., 2003, ApJ, 590, 348
Luhman K. L., Liebert J., Rieke G. H., 1997, ApJL, 489, L165
Luhman K. L., Stauffer J. R., Muench A. A., Rieke G. H., Lada E. A., Bouvier J., Lada C. J., 2003, ApJ, 593, 1093
Martín E. L., Barrado y Navascués D., Baraffe I., Bouy H., Dahm S., 2003, ApJ, 594, 525
Martín E. L., Basri G., Gallegos J. E., Rebolo R., Zapatero-Osorio M. R., Bejar V. J. S., 1998, ApJL, 499, L61
Martín E. L., Brandner W., Bouvier J., Luhman K. L., Stauffer J., Basri G., Zapatero Osorio M. R., Barrado y Navascués D., 2000, ApJ, 543, 299
Martín E. L., Zapatero Osorio M. R., Rebolo R., 1998, in ASP Conf. Ser. 134: "Brown Dwarfs and Extrasolar Planets", eds. R. Rebolo, E. L. Martín, and M. R. Zapatero Osorio The Substellar Initial Mass Function in the Pleiades. p. p 507
Maxted P. F. L., Jeffries R. D., 2005, MNRAS, 362, L45
Mermilliod J. C., 1981, A&A, 97, 235
Metchev S. A., Kirkpatrick J. D., Berriman G. B., Looper D., 2008, ApJ, 676, 1281
Miller G. E., Scalo J. M., 1979, ApJS, 41, 513
Moraux E., Bouvier J., Stauffer J. R., 2001, A&A, 367, 211
Moraux E., Bouvier J., Stauffer J. R., Cuillandre J.-C., 2003, A&A, 400, 891
Muench A. A., Lada E. A., Lada C. J., Alves J., 2002, ApJ, 573, 366
O'dell M. A., Hendry M. A., Collier Cameron A., 1994, MNRAS, 268, 181
Offner S. S. R., Klein R. I., McKee C. F., Krumholz M. R., 2009, ApJ, 703, 131
Pinfield D. J., Hodgkin S. T., Jameson R. F., Cossburn M. R., Hambly N. C., Devereux N., 2000, MNRAS, 313, 347
Pinfield D. J., et al. 2008, MNRAS, 390, 304
Rebolo R., Zapatero-Osorio M. R., Martín E. L., 1995, Nat, 377, 129
Reylé C., et al. 2010, A&A, 522, A112
Robichon N., Arenou F., Mermilliod J.-C., Turon C., 1999, A&A, 345, 471
Salpeter E. E., 1955, ApJ, 121, 161
Scalo J. M., 1986, Fundamentals of Cosmic Physics, 11, 1
Skrutskie M. F., et al. 2006, AJ, 131, 1163
Southworth J., Maxted P. F. L., Smalley B., 2005, A&A, 429, 645
Stauffer J., Klemola A., Prosser C., Probst R., 1991, AJ, 101, 980
Stauffer J. R., Hamilton D., Probst R. G., 1994, AJ, 108, 155
Stauffer J. R., et al. 2007, ApJS, 172, 663
Stauffer J. R., Schild R., Barrado y Navascues D., Backman D. E., Angelova A. M., Kirkpatrick J. D., Hambly N., Vanzi L., 1998, ApJ, 504, 805
Stauffer J. R., Schultz G., Kirkpatrick J. D., 1998, ApJL, 499, 219
Tej A., Sahu K. C., Chandrasekhar T., Ashok N. M., 2002, ApJ, 578, 523
Trumpler R. J., 1921, Lick Observatory Bulletin, 10, 110
Urban A., Martel H., Evans II N. J., 2010, ApJ, 710, 1343
van Leeuwen F., 2009, A&A, 497, 209
van Leeuwen F., Alphenaar P., Brand J., 1986, A&AS, 65, 309
Zapatero Osorio M. R., Béjar V. J. S., Martín E. L., Rebolo R., Barrado y Navascués D., Mundt R., Eislöffel J., Caballero J. A., 2002, ApJ, 578, 536
Zapatero Osorio M. R., Rebolo R., Martín E. L., 1997, A&A, 317, 164
Zapatero Osorio M. R., Rebolo R., Martín E. L., Hodgkin S. T., Cossburn M. R., Magazzù A., Steele I. A., Jameson R. F., 1999, A&AS, 134, 537

APPENDIX A: TABLE OF KNOWN PLEIADES MEMBER CANDIDATES PUBLISHED IN THE LITERATURE AND RECOVERED IN UKIDSS GCS DR9.

APPENDIX B: TABLE OF PREVIOUSLY-KNOWN PLEIADES MEMBER CANDIDATES NOT RECOVERED IN THE UKIDSS GCS DR9

APPENDIX C: TABLE OF NEW PLEIADES MEMBER CANDIDATES IDENTIFIED IN THE UKIDSS GCS DR9

APPENDIX D: TABLE OF SUBSTELLAR MULTIPLE SYSTEM CANDIDATES IN THE PLEIADES

Table A1. Sample of 1379 known Pleiades member candidates previously published in the literature and recovered in GCS DR9. We list the equatorial coordinates (J2000), GCS $ZYJHK1K2$ photometry, proper motions (mas/yr) and their errors, reduced chi-squared statistic of the astrometric fit for each source (χ^2 value), membership probabilities, and names from the literature. Note that the 312 sources without membership probabilities are divided into four groups: 190 non members (NM) detected in $ZYJHK$ but not satisfying our photometric and astrometric criteria, 42 objects without $Z+Y$ photometry (noZY), 74 objects without Z only (no$Z$), and 6 sources without Y only (no$Y$). Pleiades member candidates are ordered by increasing Right Ascension. This table is available electronically in the online version of the journal.

R.A.	Dec.	Z	Y	J	H	$K1$	$K2$	$\mu_\alpha cos\delta \pm$ err	$\mu_\delta \pm$ err	χ^2	Prob	Name
03 27 54.26	+24 56 10.9	13.808	13.400	12.820	12.255	12.005	99.999	16.62±6.95	−43.60±6.95	0.47	0.93	DH003
03 29 58.76	+23 22 18.3	13.640	13.198	12.672	12.244	11.843	11.851	21.18±3.41	−38.83±3.41	0.47	0.81	DH009
...	...	...	...	...	...	...	...	...	...	...	...	...
04 05 13.75	+24 08 42.7	14.983	14.471	13.846	13.261	12.933	12.917	19.77±3.38	−41.50±3.38	0.54	0.94	DH915
04 06 29.99	+22 33 43.6	14.376	13.856	13.201	12.623	12.273	12.269	14.83±5.07	−33.96±5.07	0.55	0.14	DH2004_916

Table B1. Coordinates (J2000) and names of 544 previously-known Pleiades member candidates not recovered in the GCS DR9. Pleiades candidates are ordered by increasing right ascension. This table is available electronically in the online version of the journal.

R.A.	Dec.	Old Names
03:27:42.06	+23:48:13.3	PELS121
03:28:01.56	+23:04:42.6	DH004
...	...	...
04:05:09.44	+23:28:59.0	DH913
04:05:13.72	+22:18:19.0	DH914

Table C1. Coordinates (J2000), near-infrared ($ZYJHK1K2$) photometry with the error bars, proper motions with errors for all new Pleiades member candidates identified in the UKIDSS GCS DR9 with the probabilistic and standard selection methods. The penultimate column gives the membership probability if the object was selected with the probabilistic method. The last column lists the source (S) of the object: "1" means that the object was identified in the probabilistic approach, "2" means that the object was identified with method #2, "12" means that the candidate is common to both selection method, and "3" means that this is a faint $YJHK$ or JHK candidate. Pleiades member candidates are ordered by increasing Right Ascension. This table is available electronically in the online version of the journal.

R.A.	Dec.	Z	Y	J	H	$K1$	$K2$	$\mu_\alpha cos\delta$	μ_δ	Prob	S
03 24 59.74	+25 34 04.5	16.878± 0.009	16.243± 0.007	15.582± 0.007	14.987± 0.010	14.606± 0.005	99.999±99.999	38.59±7.21	−49.57±7.21	—	2
03 25 30.92	+24 51 39.9	20.316± 0.126	19.478± 0.096	18.600± 0.079	18.210± 0.160	18.170± 0.120	99.999±99.999	10.72±31.33	−45.76±31.33	0.60	1
...	...	...	...	...	...	...	...	...	...		
04 10 54.54	+26 01 42.4	19.642± 0.091	99.999±99.999	17.748± 0.036	17.002± 0.027	16.417± 0.022	99.999±99.999	17.38±5.99	−47.11±5.99	0.66	1
04 11 03.84	+23 15 48.9	17.766± 0.017	17.254± 0.014	16.599± 0.014	15.986± 0.017	15.599± 0.021	15.623± 0.012	18.36±6.81	−46.34±6.81	0.61	1

Table D1. Coordinates (J2000), near-infrared ($ZYJHK1K2$) photometry, and proper motions (in mas/yr) for substellar multiple system candidates identified photometrically in the Pleiades cluster

R.A.	Dec.	Z	Y	J	H	$K1$	$K2$	$\mu_\alpha cos\delta$	μ_δ
03 25 38.73	+22 57 39.8	15.890	15.269	14.601	13.974	13.618	13.628	24.45±5.11	−47.02±5.11
03 31 20.71	+25 57 33.6	16.847	16.068	15.309	14.745	14.321	14.328	21.73±3.39	−38.42±3.39
03 32 11.55	+21 27 55.7	16.385	15.652	14.906	14.339	13.949	13.920	13.64±3.89	−40.00±3.89
03 33 49.22	+19 59 52.0	18.539	18.104	16.453	15.767	15.433	15.492	1.67±6.44	−40.37±6.44
03 34 38.61	+24 51 28.5	17.097	16.247	15.459	14.920	14.445	14.466	13.39±2.69	−37.21±2.69
03 36 01.95	+27 11 04.7	16.248	15.492	14.774	14.234	13.810	13.782	15.79±3.79	−42.70±3.79
03 36 03.85	+22 52 03.5	18.072	16.873	15.913	15.240	14.679	14.679	22.46±3.15	−46.19±3.15
03 36 53.30	+26 34 27.9	17.046	16.171	15.379	14.804	14.355	14.353	15.54±3.33	−34.04±3.33
03 40 11.98	+21 48 31.8	16.578	15.884	15.169	14.580	14.187	14.178	24.16±2.54	−40.67±2.54
03 40 45.16	+27 50 40.4	17.074	16.218	15.404	14.816	14.321	14.333	12.37±3.34	−40.37±3.34
03 40 53.66	+28 21 11.5	18.880	17.570	16.490	15.852	15.194	15.199	13.91±4.06	−31.57±4.06
03 41 40.91	+25 54 24.1	16.893	16.001	15.180	14.574	14.122	14.125	16.94±2.26	−42.13±2.26
03 41 42.41	+23 54 57.1	16.171	15.464	14.709	14.124	13.686	99.999	14.07±2.31	−47.37±2.31
03 41 54.16	+23 05 04.7	17.349	16.376	15.522	14.975	14.415	14.418	18.19±2.30	−44.74±2.30
03 43 34.49	+25 57 30.6	16.571	15.727	14.909	14.359	13.909	13.901	20.92±2.25	−47.72±2.25
03 44 14.65	+23 49 40.0	15.892	15.245	14.547	13.957	13.546	99.999	14.46±2.31	−40.15±2.31
03 44 35.16	+25 13 42.8	17.656	16.584	15.662	14.985	14.448	14.460	19.33±2.26	−44.97±2.26
03 44 35.90	+23 34 41.9	16.307	15.672	14.985	14.376	13.990	13.985	16.94±2.23	−44.39±2.23
03 45 09.46	+23 58 44.7	16.974	16.250	15.438	14.872	14.424	14.410	16.07±2.25	−42.23±2.25
03 45 31.37	+24 52 47.4	17.332	16.330	15.465	14.839	14.354	14.326	16.69±2.24	−40.30±2.24
03 45 37.76	+23 43 50.1	16.240	15.456	14.715	14.172	13.756	13.742	20.91±2.23	−45.45±2.23
03 45 41.27	+23 54 09.7	17.166	16.189	15.360	14.782	14.305	14.309	17.46±2.24	−44.47±2.24
03 45 50.66	+24 09 03.5	17.478	16.582	15.705	15.095	14.580	14.560	16.01±2.26	−40.58±2.26
03 46 05.11	+23 45 34.9	17.229	16.347	15.522	14.851	14.385	14.404	15.88±2.25	−39.21±2.25
03 46 15.11	+26 46 48.8	16.624	15.838	15.032	14.495	14.037	14.088	20.73±2.97	−42.79±2.97
03 46 20.27	+23 58 18.9	19.259	18.174	17.034	16.269	15.650	15.585	12.97±2.40	−35.00±2.40
03 46 22.25	+23 52 26.6	17.120	16.323	15.518	14.917	14.474	14.472	17.65±2.25	−38.04±2.25
03 46 26.09	+24 05 09.5	16.810	15.967	15.160	14.584	14.118	14.098	19.41±2.24	−38.71±2.24
03 46 27.10	+21 48 22.6	19.797	18.650	17.374	16.564	15.848	15.925	20.95±2.98	−48.67±2.98
03 47 11.79	+24 13 31.3	16.305	15.554	14.792	14.261	13.841	13.850	16.88±2.23	−41.27±2.23
03 47 20.48	+19 54 25.5	17.011	16.054	15.210	14.615	14.152	14.140	28.11±5.10	−39.39±5.10
03 48 04.67	+23 39 30.1	17.014	16.054	15.283	14.704	14.256	14.238	16.07±2.24	−44.27±2.24
03 48 31.53	+24 34 37.2	19.218	17.883	16.715	15.977	15.357	15.312	11.92±2.37	−46.68±2.37
03 48 35.20	+22 53 42.1	16.176	15.452	14.745	14.185	13.770	13.772	15.22±2.15	−45.62±2.15
03 48 50.45	+22 44 29.8	16.562	15.825	15.098	14.531	14.141	14.143	15.64±2.16	−42.06±2.16
03 48 57.41	+23 13 59.1	16.835	16.033	15.222	14.673	14.194	14.194	14.93±2.17	−36.62±2.17
03 50 52.17	+23 27 11.2	17.690	16.638	15.700	15.060	14.505	14.555	19.89±2.21	−41.33±2.21
03 51 38.96	+24 30 44.8	18.711	17.407	16.400	15.718	15.168	15.122	23.01±2.34	−40.47±2.34
03 53 55.13	+23 23 36.1	16.947	16.027	15.172	14.569	14.088	14.081	19.17±2.28	−44.72±2.28
03 55 27.06	+25 14 45.8	16.118	15.402	14.649	14.071	13.671	13.650	15.24±2.24	−39.66±2.24
03 56 52.31	+25 10 05.1	16.146	15.491	14.756	14.192	13.771	13.801	16.66±2.50	−38.22±2.50
03 58 00.62	+21 18 20.8	17.399	16.380	15.545	14.931	14.445	14.423	24.81±3.43	−32.13±3.43
03 58 17.43	+22 11 52.7	16.259	15.503	14.768	14.193	13.787	13.778	20.64±2.89	−34.95±2.89
03 59 59.85	+25 08 53.6	16.368	15.695	15.004	14.433	14.029	14.075	14.87±2.51	−35.69±2.51
04 00 03.21	+22 24 46.0	16.534	15.875	15.128	14.550	14.132	14.141	15.92±2.87	−33.98±2.87
04 00 08.16	+22 32 01.1	16.449	15.820	15.102	14.503	14.098	14.104	16.31±2.88	−39.63±2.88
04 00 50.52	+23 43 52.9	16.184	15.380	14.647	14.089	13.660	99.999	24.52±3.56	−40.90±3.56
04 01 28.43	+23 30 59.6	16.318	15.539	14.772	14.202	13.788	13.788	24.55±3.37	−39.20±3.37
04 01 39.83	+22 47 53.7	16.669	15.899	15.153	14.575	14.169	14.157	21.16±3.39	−42.62±3.39
04 01 50.95	+22 59 15.5	16.363	15.631	14.906	14.311	13.912	13.906	20.72±3.38	−38.98±3.38
04 09 17.80	+26 03 31.2	17.120	16.480	15.759	15.003	14.603	99.999	6.56±4.49	−33.73±4.49